



# A constant-time SLAM back-end in the continuum between global mapping and submapping: application to visual stereo SLAM



Francisco-Angel Moreno<sup>1</sup>, Jose-Luis Blanco<sup>2</sup> and Javier Gonzalez-Jimenez<sup>1</sup>

## Abstract

*This work addresses the development and application of a novel approach, called sparser relative bundle adjustment (SRBA), which exploits the inherent flexibility of the relative bundle adjustment (RBA) framework to devise a continuum of strategies, ranging from RBA with linear graphs to classic bundle adjustment (BA) in global coordinates, where submapping with local maps emerges as a natural intermediate solution. This method leads to graphs that can be optimized in bounded time even at loop closures, regardless of the loop length. Furthermore, it is shown that the pattern in which relative coordinate variables are defined among keyframes has a significant impact on the graph optimization problem. By using the proposed scheme, optimization can be done more efficiently than in standard RBA, allowing the optimization of larger local maps for any given maximum computational cost. The main algorithms involved in the graph management, along with their complexity analyses, are presented to prove their bounded-time nature. One key advance of the present work is the demonstration that, under mild assumptions, the spanning trees for every single keyframe in the map can be incrementally built by a constant-time algorithm, even for arbitrary graph topologies. We validate our proposal within the scope of visual stereo simultaneous localization and mapping (SLAM) by developing a complete system that includes a front-end that seamlessly integrates several state-of-the-art computer vision techniques such as ORB features and bag-of-words, along with a decision scheme for keyframe insertion and a SRBA-based back-end that operates as graph optimizer. Finally, a set of experiments in both indoor and outdoor conditions is presented to test the capabilities of this approach. Open-source implementations of the SRBA back-end and the stereo front-end have been released online.*

## Keywords

Bundle adjustment, computer vision, relative coordinates, stereo vision, SLAM

## 1. Introduction

*Bundle adjustment* (BA) is a well-known problem in computer vision (Triggs et al., 2000) that consists of finding an optimal estimation to the positions of a set of visual landmarks (LMs), the camera poses from where images were captured and, typically, their calibration parameters too. This problem, also known as *full SLAM* (Thrun et al., 2005) or *structure-from-motion*, is typically addressed by minimizing a single cost function that simultaneously reflects the mismatch between the LMs observed in the complete sequence of keyframes (KFs) and their predictions according to the camera pose estimates. Traditionally avoided in the mobile robotics community due to its high computational cost, BA has recently gained an immense popularity (e.g. Kaess et al., 2012; Konolige and Agrawal, 2008), due to new advances in sparse algebra (e.g. sparse Cholesky decomposition (Davis, 2006), inexact Newton-type algorithms (Agarwal et al., 2010)), becoming a promising alternative to filtering methods employed extensively

for simultaneous localization and mapping (SLAM) during previous years (Strasdat et al., 2012).

BA-based SLAM defines a graphical model where nodes are the unknowns and edges represent constraints between them. There are two kinds of unknowns: the location of a set of discrete entities observed by the sensor, called LMs, and a small fraction of all the poses (e.g. of a vehicle, a camera or a hand-held sensor) along its trajectory, called KFs. Assuming Gaussian errors for all of the observations and undertaking a least-squares criterion for the above-mentioned minimization, the process can be

<sup>1</sup>MAPIR-UMA Group, Departamento Ingeniería de Sistemas y Automática, Universidad de Málaga, Málaga, Spain

<sup>2</sup>Engineering Department, University of Almería, Spain

### Corresponding author:

Francisco-Angel Moreno, Departamento Ingeniería de Sistemas y Automática, Universidad de Málaga, ETSI Informática, Lab. 2.3.6i, Campus de Teatinos, 29071 Málaga, Spain.  
Email: famoreno@uma.es

shown to become the maximum likelihood estimator for the problem (Hartley and Kahl, 2007).

Under the general denomination of BA, different parameterizations have been proposed in the technical literature leading to the so-called *global* and *relative* BA techniques (Triggs et al., 2000). In short, global BA (GBA) selects a single KF to be the *origin* or reference frame for the coordinates of all subsequent KFs and LMs. As a consequence, a global, self-consistent map is obtained at the cost of updating all variables at every time-step. On the other hand, in relative BA (RBA), the problem unknowns are all *relative* positions between KFs and LMs. Typically, LM coordinates are defined with respect to the KF from where they were observed for the first time, while the pose of each KF is defined relative to its predecessor (Sibley, 2009). The latter feature leads to graphical models where KFs form a (mostly) linear graph, hence the motivation of naming this strategy *linear RBA* in the following. Very recently, this paradigm of relative coordinates has also been extended to work on continuous-time SLAM (Anderson et al., 2015), with basis functions used as continuous approximations of the estimated trajectory instead of relying on a sparse set of KFs.

Despite some advances, such as incremental Smoothing And Mapping (iSAM) (Kaess et al., 2008), any approach to SLAM relying on global coordinates, such as GBA, exhibits an inherent unbounded growth of the matrices involved in the graph optimization as the explored area becomes larger and longer loops are closed. Therefore, in principle, none of those SLAM methods could be practical for any robot aimed at life-long exploration. RBA approaches aim at solving that scalability issue (Sibley et al., 2010a), since they only optimize a local region of the graph around the latest KF (i.e. the current camera pose), hence achieving a bounded computational cost by definition. However, as will be discussed later, the information matrices involved in RBA formulation become less sparse than their GBA counterparts, hence preventing it to fully exploit sparse algebra techniques and, consequently, to achieve an optimal performance.

The present work claims and shows that the sparsity level in such matrices can be controlled by changing the way in which relative coordinates are defined, which in turn determines how nodes are linked to each other within the graph. In particular, the creation of conveniently connected *submaps* leads to sparser matrices than those in standard RBA approaches, without compromising their scalability advantages with respect to their global counterpart. This flexibility allows us to derive a continuum of strategies from linear RBA to submapping with local maps. This is the essence of the so-called *sparser* relative bundle adjustment (SRBA) method, preliminarily introduced by Blanco et al. (2013), and now presented here in the context of a complete SLAM framework, tested with real datasets.

SRBA advocates the creation, within the graph, of relative submaps whose origin KFs are mostly linearly

connected, thus defining *shortcuts* between nodes. This introduces zero blocks in the matrices involved in the optimization (i.e. Jacobians and Hessians), hence becoming sparser. By following the strategy of optimizing only the graph around the current KF, also found in linear RBA, SRBA ensures bounded-time graph optimization, even in the event of closing loops of arbitrary length. However, we claim that different connection patterns allow for the optimization of larger map areas for *any* fixed maximum topological distance from the current KF. Finally, a *shortest-path spanning tree* (required by graph search operations during optimization) is incrementally maintained up to a certain topological distance using the novel *constant time* algorithm which was also introduced by Blanco et al. (2013).

In summary, the present work extends our preliminary results on SRBA and presents the following contributions.

- The SRBA bounded-time nature is demonstrated by providing detailed pseudo-code listings and thorough complexity analyses for the most important algorithms that are performed on the graph.
- We provide an experimental validation, with real datasets in different conditions, of the SRBA back-end as graph optimizer, applied to stereo visual SLAM.
- A front-end is developed that seamlessly integrates several state-of-the-art computer vision techniques, along with a decision scheme for KF insertion. This includes all of the necessary elements to build, along with our SRBA back-end, a complete stereo visual SLAM system.

Regarding the latter point, the proposed front-end is constructed upon the following building blocks. Keypoint detection and description is accomplished through the ORB method (Rublee et al., 2011), which provides features invariant to scale and rotation with associated binary descriptors. A binary *bag-of-words* (Galvez-Lopez and Tardos, 2012) for ORB descriptors is employed to assist data association by restricting the search area when looking for loop closures, hence boosting the overall performance. Ego-motion estimations between consecutive frames are computed through our visual odometry method proposed in Moreno et al. (2013), a fast and reliable outlier detector based on robust kernels, as an efficient alternative to random sample consensus (RANSAC). Finally, we have devised a decision scheme based on image similarity and geometrical distance between KFs to decide when to add new KFs to the graph, aiming to keep it as small as possible.

Our proposal is supported by a set of experimental results with synthetic and real images recorded in both indoor and outdoor conditions. A video of such experiments can be watched at <https://goo.gl/1Ap4p9> and the source code is available on-line.<sup>1</sup>

## 2. Related work

BA has undergone a rebirth as an attractive solution to the SLAM problem, thanks to the incorporation of recent sparse algebra techniques. This has turned it into a strong alternative to probabilistic filtering, which had become the standard for real-time vision-based SLAM and global localization during the last decades, leading to a long list of works which can be found elsewhere (e.g. Blanco et al., 2010; Civera et al., 2007; Moreno et al., 2009; Wolf et al., 2002). A thorough comparison between filtering and BA solutions is presented in Strasdat et al. (2010) and Strasdat et al. (2012), ultimately advocating for the application of BA as it outperforms filtering methods in terms of accuracy per unit of computation time.

Different techniques have been proposed to reduce the computational burden of general BA solutions, which quickly increases as the size of the map grows. For instance, the well-known PTAM method (Klein and Murray, 2007) separates camera tracking and mapping in two parallel threads and performs KF-based global BA by optimizing the graph over a subset of the  $N$  most recent camera poses, in order to achieve real-time performance. However, its effectiveness is limited to small indoor scenarios and does not scale well with large environments.

Another notable approach to SLAM is iSAM (Kaess et al., 2008), where a factored representation of the approximate Hessian matrix is exploited to provide easy access to the marginal covariances needed for data association. This matrix is incrementally updated and maintained sparse by reordering the involved variables.

On the other hand, there are several proposals that adopt a relative formulation, often in combination with other techniques such as *submapping* or data marginalization, in order to reduce the problem complexity and to achieve a bounded-cost performance that can lead to on-line, real-time operation, as claimed in several works (e.g. Eade and Drummond, 2008; Konolige and Agrawal, 2008; Lim et al., 2011; Sibley, 2009; Sibley et al., 2009, 2010a).

A hybrid metrical-topological world representation was successfully proposed in Blanco et al. (2008) within a Bayesian framework, as a natural mechanism to deal with the map scalability issue. In the context of BA, the work of Lim et al. (2011) proposes a hybrid metrical-topological representation of the map which provides scalability to the BA problem. This proposal benefits from the topological map properties to allow for instant loop closures while metric locally consistent maps are maintained by embedding neighbor KFs and LMs into a single Euclidean space and optimizing over the submap. The submaps are then treated as rigid bodies in a global adjustment process that yields a globally consistent map, although this last step is not performed in real-time.

In Konolige and Agrawal (2008), a *skeleton* is built from the camera and LM relative poses, in order to represent a reduced system that approximates the full problem, leading

to feasible solutions when dealing with large loop closures. This skeleton is formed by marginalizing features over camera poses and subsequently further reducing the latter.

The work in Sibley (2009) and Sibley et al. (2009) constitutes the basis of the RBA approach developed in this paper, being further extended in Sibley et al. (2010a), where a sliding window filter (SWF) based on a delayed state marginalization is proposed. Its operation ranges from extended Kalman filter (EKF) to full SLAM according to the window size, while performing both LM and camera pose marginalization to achieve constant time operation, demonstrating similar convergence properties to the full batch solution and outperforming those from standard visual odometry. Nevertheless, it has been specifically devised for EDL (entry, descent and landing) applications for autonomous landing vehicles and there is not any validation in more general situations as typical indoor and outdoor urban environments. These scenarios, though, have been addressed by Sibley (2009) and especially by Sibley et al. (2010b), where a large set of outdoor experiments have been conducted to demonstrate the scalability potential of relative approaches. Among them, it can be highlighted the estimation of a 121-km outdoor path from Oxford to London that includes the use of different forms of transport such as walking, bikes, trains and some others.

Recently, Mur-Artal et al. (2015) presented a visual SLAM system which has some similarities with the present work. They also addressed BA by relying on ORB features for tracking, mapping and performing place recognition based on bag-of-words. Since it operates on monocular images, it is provided with an automatic procedure for map initialization that includes the parallel computation of both an essential matrix and a fundamental matrix to infer the relative pose between two frames, regardless of the type of scene. Once computed, one of them is heuristically selected and the pose is derived from it. Our work does not need such procedure as we employ stereo images that provide immediate 3D information for the map initialization. Apart from this, the main difference with our approach comes from the fact that they optimize a reduced graph, denoted by *essential graph*, which contains all of the problem KFs but a reduced number of edges. Our work, in contrast, relies on the optimization of the local area of the graph, which includes the current and nearby submaps (up to a certain topological distance) and all their associated edges, building a locally consistent map.

In comparison with the above-mentioned methods, in this paper we adopt an approach that, instead of being attached to a single strategy, defines a continuum of solutions that range from global BA to linear RBA (e.g. Sibley et al., 2009). This flexibility is derived from a submapping scheme that allows us to exploit more thoroughly the inherent sparsity of the system matrices without performing data marginalization. The so-called *sparser* RBA will be explained in Section 5.

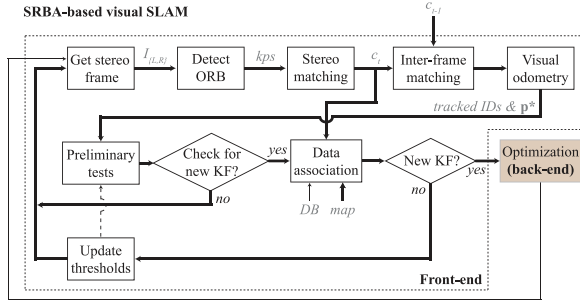


**Fig. 1.** Scheme of the proposed SRBA-based visual SLAM system, with the focus on the front-end structure.

### 3. System overview

This section describes the proposed system built upon ORB keypoints and SRBA to perform visual SLAM. It can be split into a front-end, which is in charge of extracting and matching features from the input stereo images, performing visual odometry between consecutive time-steps and, if needed, finding correspondences between the current observation and the map, and a back-end that creates, manages and performs inference on the graphical representation of all of the unknown relative camera poses and LM positions as the robot navigates.

At the core of our proposed front-end is the ORB feature detector (Rublee et al., 2011). Relying on the FAST and BRIEF methods, ORB is not only a fast and reliable feature detector but it also provides binary descriptors for the keypoints, which are efficiently matched by measuring Hamming distances. Data association is aided by the management of an image database based on a binary bag-of-words (Galvez-Lopez and Tardos, 2012). When data association is needed, the set of descriptors associated to the keypoints extracted in an image is employed to query the database looking for the most similar image stored in it, thus leading to the process of matching features between the current observation and the stored map.

Regarding the back-end, the proposed SRBA method models the entities in the SLAM problem as a graph, whose nodes are KFs and LMs while the edges symbolize the relative constraints between them. In order to estimate both the world structure and the KF poses, a nonlinear least-squares optimization process is carried out, which minimizes the mismatch between all of the observed image features and their predicted positions in the image. In general, such an error function is assumed to be quadratic in the image feature projection errors, though non-quadratic error functions, sometimes referred as *robust kernels*, can be chosen to deal with the presence of outliers in the observations. Huber kernels are typically used to this end, although recent quantitative benchmarking has demonstrated that other kernels achieve superior performance in photogrammetric and computer vision applications (Concha and Civera, 2015). It must be noted that, by disregarding the estimation of LM positions, we can follow a simplified version of the

above optimization process to estimate the camera ego-motion between consecutive time-steps, i.e. to perform *visual odometry*.

Figure 1 shows the general scheme of the proposed system, sketching all the stages from the acquisition of the stereo images to the joint estimation of LM positions and robot poses up to the current time-step, carried out by the back-end. Note that the procedures included in our front-end have been emphasized in this figure, since they will be explained next. The back-end, represented here as a shaded block, is addressed later in Section 5.

#### 3.1. Notation

Formally, let us define the system state vector as

$$\mathbf{s} = (\mathbf{p}, \mathbf{x}) \quad (1)$$

which encompasses the problem unknowns, i.e. the collection  $\mathbf{p}$  of  $P$  KFs and the set  $\mathbf{x}$  of  $L$  3D LM positions:

$$\begin{aligned} \mathbf{p} &= \{\mathbf{p}_{j,b}\}_{j=1\dots P, b \in \{1\dots P\} | b \neq j} \\ \mathbf{x} &= \{\mathbf{x}_{j,b}\}_{j=1\dots L, b \in \{1\dots P\}} \end{aligned} \quad (2)$$

For the KFs, this notation defines  $j$  as an identifier for the KF while  $b$  indicates the index of the reference frame which it is referred to. Note that  $b$  cannot be the same as  $j$  since it does not make sense to refer a KF to its own reference system. Regarding LMs,  $j$  stands again for an identifier while  $b$  specifies the so-called *base* KF, which is the reference frame in which the  $j$ th LM coordinates are expressed. It is important to remark that the choice of *which* KF will be the reference KF  $b$  represents the main difference between global and relative approaches, i.e. in global SLAM there exists a privileged coordinate frame that serves as a reference for the entire map.

Let  $\mathbf{z}$  be the set of  $N$  observations gathered at a certain time-step, each one assumed to be corrupted by zero-mean Gaussian noise with information (inverse covariance) matrix  $\Lambda_j$ :

$$\mathbf{z} = \{\mathbf{z}_j^o\}_{j=1\dots N, o \in \{1\dots P\}} \quad (3)$$

where  $j$  represents the index of the observed LM, and  $o$  stands for the index of the current KF, which will be called the *observer* KF.

In this paper, the observations are represented by 4D vectors comprising the image coordinates of the 3D LM projections in both the left and right images:

$$\mathbf{z}_j^o = (u_L, v_L, u_R, v_R)_j^T \quad (4)$$

Finally, let  $\mathbf{T}_{b,o} \in \mathbf{SE}(3)$  denote a  $4 \times 4$  transformation matrix that represents the pose of the  $o$ th KF with respect to the  $b$ th KF, its reference system. Thus, the conversion of the  $j$ th LM coordinates, referred to its base KF  $b$ , to its coordinates with respect to a certain observer KF  $o$  is performed through

$$\mathbf{x}_{j,b}^o = (\mathbf{T}_{b,o})^{-1} \mathbf{x}_{j,b} \quad (5)$$

In relative formulations, this matrix is built from a chain of transformations, becoming the main responsible for the loss of sparsity: we continue this discussion in Section 5.

For the sake of clarity, the subscript and superscript concerning the base and/or the observer KFs for the KFs, the LMs and/or the observations will be omitted whenever they are unnecessary.

## 4. Front-end

This section describes the methods implemented within the system front-end, from keypoint detection in a pair of stereo images to the extraction of a set of associated visual features between the current observation and the stored map.

### 4.1. ORB keypoints

Due to computational efficiency requirements, feature-based visual SLAM frameworks tend to rely on efficient methods to detect keypoints and extract descriptors that are fast to both compute and match. As a result, *binary* detectors and descriptors are becoming a standard. In this paper we employ the OpenCV (Bradski, 2008) implementation of the ORB (Rublee et al., 2011) keypoint detector and descriptor.

Built upon the FAST detector (Rosten and Drummond, 2006) and the BRIEF descriptor (Calonder et al., 2010), ORB enhances them by providing scale and rotation invariance to the detected keypoints. Stereo matching is subsequently performed through the Hamming distance (Hamming, 1950) between ORB descriptors, i.e. counting the number of different bits between them. We also consider epipolar restrictions which, in this case, reduce to corresponding points lying on the same image row. The set of stereo matches at  $t$ th time-step is denoted by  $c_t$ .

Finally, in order to provide tracking information to later stages in the system, a unique ID is assigned to every stereo match in  $c_t$ .

### 4.2. Visual odometry

Camera ego-motion between the previous time-step and the current one is then estimated by the visual odometry method we formerly presented in Moreno et al. (2013).

First, *inter-frame* keypoint correspondences are found between the current stereo matches and the previous ones ( $c_t$  and  $c_{t-1}$  in Figure 1, respectively). Following a similar approach than that for stereo matching, we look for potential correspondences between the current left image and the previous one, relying again on descriptor distances and epipolar restrictions (which, in this case, involves the computation of the fundamental matrix for the considered images). For the sake of robustness, this process is repeated for the right images so that only the matches consistent with those found in the left ones are kept.

Visual odometry is then computed following the general approach of iteratively minimizing a certain cost function

which measures at each iteration the mismatch between the predicted and the observed image projections of corresponding keypoints at both time-steps:

$$F(\mathbf{p}) = \sum_i \frac{1}{2} \Delta \mathbf{z}_i^T \Lambda_i \Delta \mathbf{z}_i \quad (6)$$

where  $\mathbf{p}$  stands for the estimation of the camera pose change between time-steps  $t - 1$  and  $t$  and represents the only unknown within the system state in Equation (1) for visual odometry. In this situation, therefore, the keypoints 3D coordinates are considered to be fixed, and are computed by back-projecting their image coordinates at time  $t - 1$ .

On the other hand,  $\Delta \mathbf{z}_i = \bar{\mathbf{z}}_i - \mathbf{z}_i$  stands for the error between the prediction  $\bar{\mathbf{z}}_i$  of the  $i$ th feature and its observation  $\mathbf{z}_i$ . The *prediction function* determines the coordinates of a keypoint in the current image according to its 3D position  $\mathbf{x}$ , and the estimation  $\mathbf{p}$  at the current iteration:

$$\mathbf{h}(\mathbf{p}, \mathbf{x}) = \bar{\mathbf{z}} = \{\bar{\mathbf{z}}_i\}_{i=1, \dots, N} \quad (7)$$

Finally,  $\Lambda_i$  in Equation (6) is an appropriate weighting matrix, proportional to the inverse covariance of the zero-mean normally distributed noise (with a standard deviation of  $\sigma_p$ ) that affects keypoint locations. Assuming identical error distributions for all detected features in both  $u$  and  $v$  directions leads to the simplification  $\Lambda_i = (1/\sigma_p^2) \mathbf{I}$ ,  $\forall i$ .

Typically, the cost function is minimized by computing small increments  $\Delta \mathbf{p}$  that are added to the current estimation until convergence, yielding a final solution  $\mathbf{p}^*$ . These increments can be found by solving the well-known Gauss–Newton equation:

$$\begin{aligned} \mathbf{H} \Delta \mathbf{p} &= -\mathbf{g} \\ (\mathbf{J}^T \Lambda \mathbf{J}) \Delta \mathbf{p} &= -\mathbf{J}^T \Lambda \Delta \mathbf{z} \end{aligned} \quad (8)$$

where  $\mathbf{J} = \partial \mathbf{h}_z / \partial \mathbf{p}$  stands for the Jacobian matrix of the prediction function, and  $\Delta \mathbf{z}$  is a block-column vector containing the errors  $\Delta \mathbf{z}_i$  of the individual observations.

However, the quadratic cost function in Equation (6) is not robust against the presence of outliers, so that the minimization process may converge to an invalid solution. Thus, we follow the ERODE method presented in Moreno et al. (2013) which, instead, proposes the use of a robust cost model based on the pseudo-Huber function (Huber and Ronchetti, 1981):

$$F_r(\mathbf{p}) = \sum_i \frac{1}{2} \left[ 2b^2 \left( \sqrt{1 + \left( \frac{s_i}{b^2} \right)^2} - 1 \right) \right] \quad (9)$$

with  $b$  being a parameter which tunes the shape of the function and  $s_i = \Delta \mathbf{z}_i^T \Lambda_i \Delta \mathbf{z}_i$ . Using this function also implies a change in the Gauss–Newton expression shown in Equation (8), which becomes

$$(\mathbf{J}^T \Lambda \mathbf{J}) \Delta \mathbf{p} = -\rho' \mathbf{J}^T \Lambda \Delta \mathbf{z} \quad (10)$$

---

**Algorithm 1.** New keyframe decision scheme.
 

---

**Input:**  
 $\mathbf{IDs} = \{ID_1, \dots, ID_{n_t}\}$   $\triangleright$  IDs of the  $n_t$  tracked keypoints  
 $\mathbf{p}^*$   $\triangleright$  Estimated pose change from visual odometry  
 $\mathbf{c}_p$   $\triangleright$  Accumulated pose change, updated from the last call to this algorithm

**Output:**  
 $d$   $\triangleright$  Decision about whether or not create a new keyframe  
 $\mathbf{c}_p$   $\triangleright$  New accumulated pose change

```

1:  $\mathbf{c}_p \leftarrow \mathbf{c}_p \oplus \mathbf{p}^*$   $\triangleright$  Update the current estimated pose change
2: if  $|\mathbf{c}_p| > th_1$  OR  $n_t > th_2$  then
3:    $\mathbf{IDs} \leftarrow \emptyset$   $\triangleright$  Reset tracked IDs
4:    $\mathbf{c}_p \leftarrow \mathbf{O}$   $\triangleright$  Reset to a zero pose change
5:    $d \leftarrow \text{true}$   $\triangleright$  Create a new keyframe
6: else
7:    $d \leftarrow \text{false}$   $\triangleright$  Do not create a new keyframe
8: end if
return  $\{d, \mathbf{c}_p\}$ 
    
```

---

where  $\rho' = \{\rho'_i\}$  is a block-column vector with the derivative of the pseudo-Huber function for each observation:

$$\rho'_i = \frac{\partial}{\partial s_i} \left[ 2b^2 \left( \sqrt{1 + \left(\frac{s_i}{b}\right)^2} - 1 \right) \right] = \frac{1}{\sqrt{1 + \frac{s_i^2}{b^2}}} \quad (11)$$

Adopting this procedure, the contribution in the cost function of the large errors introduced by the outliers is significantly mitigated. This approach implies that all input data are considered in the minimization process but, on the other hand, there is no need to try different hypotheses of the model (as with RANSAC). With this method, the estimation process naturally converges towards the true solution and, after a few iterations, the outliers appear clearly visible in the vector of residuals so that we can remove them and, subsequently, refine the estimated solution to achieve higher accuracy.

It is important to remark that, although visual odometry is computed at every time-step, we follow the usual practice in the computer vision and SLAM literature of not creating KFs so often, but only when a set of conditions are fulfilled, as explained next.

### 4.3. KF creation decision

Creating new KFs is a computationally expensive process. It implies inserting new variables and constraints in the graph, then optimizing the whole system or part of it. This is specially noticeable when working with real data, since the number of features detected in images may become considerably large. However, in our previous work (Blanco et al., 2013) little attention was paid to this issue, since we focused on synthetic, sparse maps. In this work, on the contrary, a set of heuristics has been defined to decide when to create new KFs, following the common idea of inserting a new one only when the explored area is becoming different enough from the last stored KF.

Algorithm 1 summarizes our proposed scheme for deciding when to create KFs. The process starts from the visual odometry output, which consists of: (i) a list comprising the IDs of the tracked keypoints (assigned during stereo matching) and (ii) the estimation of the pose change between consecutive time-steps  $\mathbf{p}^*$ . The former is employed to keep track of the IDs assigned to the keypoints that have been correctly associated between consecutive time-steps. The drop of the number  $n_t$  of tracked keypoints below a certain threshold indicates that the observed scene is becoming significantly different. The latter, in turn, is employed to incrementally build a vector  $\mathbf{c}_p$  that stands for the transformation between a certain camera pose and the one at the current time-step. Thus, as the camera moves,  $\mathbf{c}_p$  incrementally grows in terms of translation and/or rotation. When such translation or rotation grow above some pre-defined thresholds, the camera is considered to have substantially moved from the previous KF and, therefore, it might be observing a significantly different area.

Any of these two indicators will trigger a data association process that will ultimately confirm whether or not the current observation has little in common with the system knowledge of the environment. In any case, both the monitored incremental pose  $\mathbf{c}_p$  and the IDs of the tracked keypoints are reset, as the decision scheme will be started again from the beginning. Data association is discussed in Section 4.4.

In this paper, the number of associated visual features yielded by data association is employed as a measure of the similarity between the compared KFs. Thus, if such number falls below a certain threshold (refer to Figure 1), a new KF is created with the information extracted from the current pair of images. Otherwise, the present observation is considered to still share sufficient information with the most similar KF observed up to the current time-step, hence discarding the addition of a new KF. Finally, the thresholds employed in the preliminary tests are adjusted taking into account the number of associated visual features. Hence, the translation and rotation limits allowed before triggering a new data association process reduce as the measured similarity decreases.

### 4.4. Data association

One of the key stages in the design of SLAM systems is the so-called *data association*. This term stands for the process of looking for correspondences between the current observation and the knowledge that the system has about the environment, i.e. the map. We refer interested readers to a more in-depth discussion of the problem presented elsewhere (Blanco et al., 2012). A special situation of paramount importance arises when the current observation matches to LMs stored some time ago, hence implying a re-observation of an already explored area. This situation is known as *loop closure*.

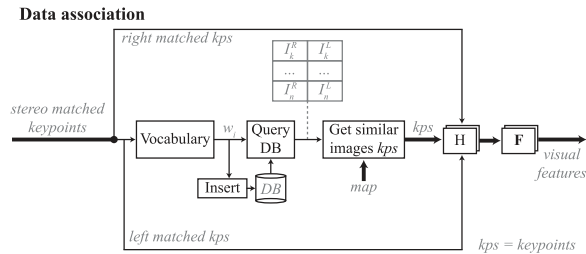


**Fig. 2.** Scheme of our proposed data association procedure. Matched ORB keypoints ( $kps$ ) from the left image are converted into a vocabulary word  $w_i$  employed to query (and which is subsequently inserted into) the image database (DB), retrieving a list of similar images. Then, current left and right keypoints are matched against those from the retrieved similar images by means of the Hamming distance between their descriptors (H blocks). Fundamental matrices  $\mathbf{F}$  are finally employed to discard outliers.

In this work, data association follows the approach of the above-explained inter-frame matching process and extends it by introducing a previous stage that selects the most similar KF to the current one among those already stored in the graph. This stage aims at detecting loop closures and also relies on the ORB descriptors computed during keypoint detection to identify the corresponding observed LMs, as depicted in Figure 2.

We adopt a bag-of-words approach based on such binary descriptors to efficiently cope with this problem. The basic technique underlying a bag-of-words approach consists of building a database from the images recorded as the camera moves, then finding the most similar one within the database when a new image is captured. Specifically, we employ the method presented in Galvez-Lopez and Tardos (2012), which was initially developed for BRIEF descriptors, but that has also proven to perform well with ORB descriptors because of their similarity.

In short, the bag-of-words technique uses a previously built visual vocabulary to transform an image to a numerical vector that is subsequently employed to look up among the images stored in the database. Since the bag-of-words presented in Galvez-Lopez and Tardos (2012) is hierarchical, the vocabulary structure becomes a tree.

A schematic view of the different stages carried out in this paper to perform robust and reliable data association is shown in Figure 2. There, it can be seen how, by using the pre-built word vocabulary, all the ORB descriptors extracted from an image (we only employ the left image) are summarized into a single word  $w_i$  that is subsequently stored within the database. As new images are captured, the so-obtained words are employed to query the database, retrieving this way a small list containing the most similar images within it. Therefore, the query result restricts the search for correspondences between individual LMs to only those belonging to the most similar images instead of the whole map.

Once the most similar stereo images are retrieved, their keypoints and those from the current image pair are matched following the inter-frame matching process explained in Section 4.2, yielding a set of associated visual features which will represent the input of the SRBA-based back-end. Finally, in order to consider an association as valid, all of the matched projections of the LM in the four images must be consistent with the epipolar geometry and the distance between their descriptors must fall below a threshold. This methodology reduces the presence of outliers in the data association output.

It is important to note that, as the camera explores unknown areas, the most similar image will be the last one inserted into the database, but, when visiting already explored zones, older images will be also retrieved, hence detecting loop closures.

## 5. Back-end

As already introduced in previous sections, one can establish two main variations of BA techniques, also known as *smoothing* methods (Strasdat et al., 2010), according to the representation chosen for KFs and LMs: GBA and RBA. The principal differences between them is that GBA builds a global map by imposing a privileged KF to be the *origin* of coordinates, whilst RBA only estimates relative coordinates between KFs and LMs.

The main drawback of GBA that motivates the use of *relative* approaches to BA lies on the computational burden that global formulations suffer when dealing with large graphs, especially during loop closures. In theory, the number of unknowns that may need to be updated during a loop closure in GBA is *unbounded*. Relative methods, on the other hand, optimize only a small part of the graph, leading to smaller optimization problems which can be handled efficiently in *bounded* time. However, the matrices associated with those smaller problems are significantly denser than their global counterparts due to the need to perform chains of pose compositions at each observation, since the coordinates of the stored LMs (referred to their base KF) have to be transformed to the current observer KF.

There exist two important concepts which are unique features of RBA and do not have a counterpart in GBA or global SLAM.

- Maximum topological distance ( $D_{max}$ ) for local map optimization. This parameter defines how far from the current KF should we optimize at each time-step, i.e. it determines the extension of the “active part” of the map. Implicitly, this parameter also sets the minimum distance between the base KF of observed LMs and its current observer KF for it to be considered a loop closure.
- Shortest-path spanning trees (STs) for every KF. These are data structures required to efficiently find the shortest paths between any pair of KFs within a distance  $D_{max}$ . These paths are needed to determine the

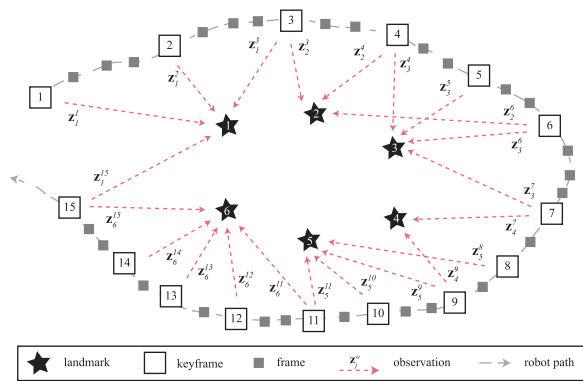


**Fig. 3.** Example of a BA problem.

variables involved in the chains of pose compositions employed to transform LM coordinates and to determine what observations may be considered loop closures. A constant-time algorithm for incrementally updating STs over time was proposed in Blanco et al. (2013) and will be summarized later.

As a consequence of optimizing only a part of the graph, RBA approaches create maps that are only locally consistent. Nevertheless, we claim that local maps of an environment, which include a correct representation of its global topological structure, are perfectly suitable for most common mobile robot operations, such as autonomous navigation via path planning and obstacle avoidance. Regarding the claims made elsewhere (Kaess et al., 2012) about the unsuitability of relative graphs for finding potential *shortcuts* during exploration, we believe that, provided that errors in the estimated relative poses between local maps are reasonably reduced, relative coordinates have enough accuracy to perform such operations. Notice that relative coordinates for KFs farther than  $D_{max}$  can be obtained at any instant by simply chaining the poses of edges along a ST rooted at some KF in the area of interest. That is, any efficient global SLAM method (such as iSAM2 in Kaess et al. (2012)) can be used to retrieve the global map from the relative graph built by RBA, although it would normally not be required for any robot operation.

SRBA (Blanco et al., 2013) was proposed as a blended solution in between GBA and the linearly connected implementation of RBA described above. By changing the policy about how to create new edges, SRBA introduced the idea of defining some KFs as *origin* KFs, dynamically selected as local reference systems and effectively creating *submaps*. Poses of all KFs within a submap are referred to its origin KF, whereas LM coordinates are referred to the KF where they were observed for the first time, as usual in RBA. The underlying idea of this submap-based representation is to generate edges between origin KFs so that paths between KFs become shorter in average, thus reducing the loss of sparsity that linear RBA incurs in, while keeping its advantages over global mapping.

In order to illustrate the differences between the aforementioned approaches, we refer to the example scenario represented in Figure 3. There, a robot follows an arbitrary path through an environment while gathering a total of 22 observations (shown as red-dashed arrows) of the 6 LMs present in the scenario (displayed as numbered stars). In the figure, the observations are labeled following the notation introduced in Equation (2). During navigation, 15 KFs have been defined among the whole set of captured frames.

In this situation, GBA defines all of the KF poses and LM positions referred to the global reference system centered at KF#1, as shown in Figure 4 (top). Consequently, all of the observations obtained from KFs different from KF#1 imply the transformation of the LM global coordinates to the KF local reference system, hence inserting a non-zero block into the Jacobian matrix corresponding to the pose of the current observer KF. As a result of the global representation of KFs, this implies that  $\mathbf{T}_{b,o}$  in Equation (5) is composed by only one transformation with  $b = 1$  for all of the observations gathered from KFs different to the first one.

On the other hand, in linear RBA, the global poses of the KFs are not the unknowns of the problem, but, instead, the relative transformations between them are. Usually, the defined edges link consecutive nodes creating linearly connected graphs, while LMs are defined with their coordinates referred to the KF where they were observed for the first time, as shown in Figure 4 (middle). In addition to that, another difference with GBA arises when the camera closes the loop, so that the problem structure must be modified due to the addition of a new unknown: the edge that joins the current KF and the *old*, re-visited one (please, refer to the green dotted edge in Figure 4 (middle) joining KF#15 and KF#1).

As a negative side effect, the sparsity level of both the Jacobian and the Hessian matrices results in fact reduced, degrading the efficacy of sparse algebra methodologies. This relative formulation leads to  $\mathbf{T}_{b,o}$  in Equation (5) becoming a chain of pose compositions following the path along the edges between the observer and the base KFs, inserting dense blocks of size  $L \times L$  in the matrices, with  $L$  being the number of edges between both KFs along the shortest path.

However, the potential of RBA lies on its flexibility, since it allows the optimization of only a subset of the problem unknowns, chosen according to the area affected by the current observation. This area is often called the *active region* and it is built through a breadth-first-search starting at current KF where the re-projection errors are computed in each KF, being added to the active region those with errors above a defined threshold. Moreover, those LMs observed from the current KF are also considered to be part of the active region.

In addition, the active region is augmented by another set of KFs called the *static region*, which is composed by



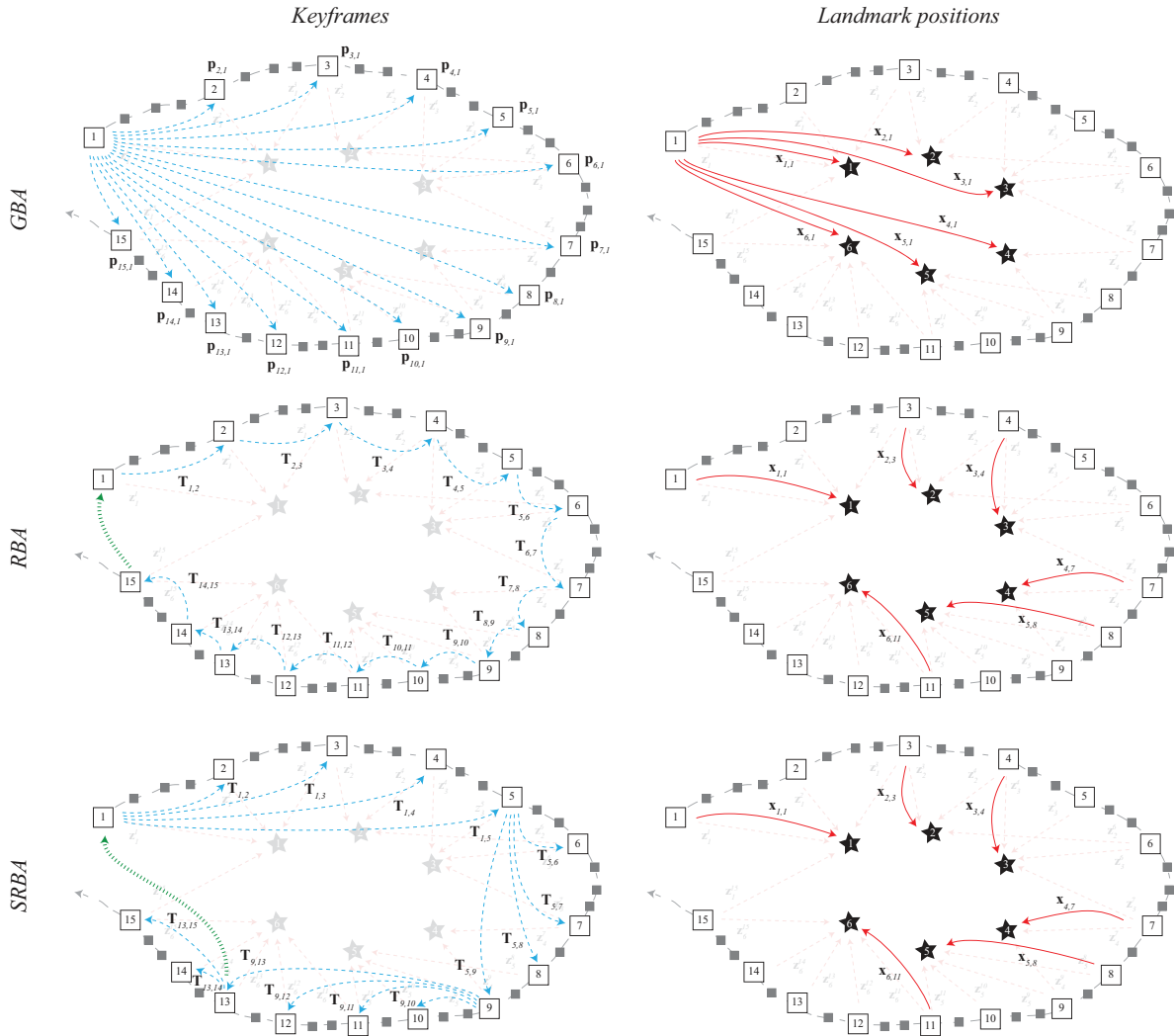


**Fig. 4.** Graph representation under a GBA (top), linear RBA (middle) and SRBA (bottom) approaches. Blue dashed arrows represent edges between KFs and their origins, while red solid arrows indicate LM positions with respect to their base KFs. For SRBA, the number of KFs within each submap has been set to 5.

any non-active KFs that have measurements of the currently observed LMs. The measurements at the static KFs are included in the least-squares minimization but their relative positions are not optimized in the process, hence the term *static*.

Since only the unknowns involved in the active region are optimized in RBA, the Jacobian and Hessian matrices become significantly smaller and, more importantly, the complexity burden of the solution remains bounded even in the presence of large loop closures. Fixed and adaptive versions of the active region can be found in Sibley (2009) and Sibley et al. (2009), respectively.

Regarding SRBA, a possible graph created under this framework for such scenario is shown in Figure 4 (bottom). Note how the graph has been divided in four submaps of size 5 whose origin KFs are those numbered 1, 5, 9 and 13. All of the KFs within the submaps are referred to their

origin KF and, similarly to the RBA case, their pose transformations with respect to it have been labeled by  $T_{j,b}$ , with  $j$  standing for the KF index and  $b$  representing its reference frame (or origin KF). On the other hand, LM positions  $x_{j,b}$  are represented following the same convention as for the standard RBA approach, with their coordinates referred to their base  $b$  KF. Both the poses of the KFs and the positions of the LMs define the system state (i.e. the problem unknowns), to be determined from the observations, as in any BA problem.

It can be seen in the figure that edges between origin KFs have been created (e.g. from KF#1 to KF#5) so that when the coordinates of a LM have to be transformed from its base KF  $b$  (member of submap  $s_i$ ) to the observer KF  $o$  (member of submap  $s_j$ ), the corresponding chain of poses only involves the existing edges between the origin KFs of the traversed submaps (from  $s_i$  to  $s_j$ ) in addition to those

between KFs  $b$  and  $o$  and their respective submap origins. Generally, such path across the graph will be shorter than the chain of poses stated by standard linearly connected RBA, being this effect more beneficial for larger submaps. Thus, this approach may be intuitively understood as a way of creating *shortcuts* in the pose graph to shorten paths along KFs chains, therefore reducing  $L$  and leading to sparser matrices, as shown later.

It is important to note that, by setting up submap sizes from 1 to infinity, SRBA seamlessly integrates all of the possible KFs configurations ranging from pure linear RBA to GBA, proving the flexibility of this blended approach.

### 5.1. Back-end implementation

As explained in Section 4.3, once the decision to insert a new KF has been taken, the set of visual features obtained through data association are fed to the SLAM back-end to maintain and optimize the graph that represents the relative map of SRBA.

The entry point for the back-end, summarized as pseudocode in Algorithm 2, takes the set of observations (and their data association) for the current KF, expands the graph as needed to accommodate the new KF, determines whether one or more KF-to-KF edges have to be created (the latter case corresponds to a loop closure) and optimizes the so-obtained nearby variables to ensure a consistent local map around the current KF. Subsequent subsections address, from a top–bottom perspective, each of the sub-algorithms required to perform all of these tasks. Refer to Table 1 for a summary of the notation employed in all of the algorithms. Worst-case computational complexities are summarized along with the pseudo-code, in order to provide a validation of the bounded-time nature we claim for SRBA. Please, refer to Blanco-Claraco (2013) for further low-level details about the C++ structures mentioned in these algorithms.

From the computational cost analysis of our method, we can conclude that each time step has a typical cost that grows with the cube of  $N_R$  (the number of reachable KFs from any other KF within a maximum topological range of  $D_{max}$ ) and linearly with  $N_o$  (the number of observed LMs). Note that  $N_R$  is bounded, as long as it is the degree of the graph. A key issue here is modeling the number of edges (not nodes) within  $D_{max}$ . Assuming a constant ratio  $\gamma$  between edges and nodes, we have  $O(\gamma N_R)$  edges to optimize in each time-step (line 8 in Algorithm 2).

To achieve minimal computational cost,  $N_R$  should be as reduced as possible, which involves having a sparsely connected graph. Nevertheless, the larger  $N_R$  is, the larger the number of KFs and LMs of the map that are kept locally consistent. On the other hand, it is also desirable to decrease  $L$  (topological path length between observer KF and base KF) as much as possible, since it leads to smaller dense blocks in the approximate Hessian matrix. However this

**Table 1.** Summary of notation employed in the algorithms.

Symbol	Description
$D_{max}$	Maximum depth of maintained STs
$N_R$	The order of how many KFs are reachable within a range of $D_{max}$
$N_o$	Number of observations in a timestep
$N_{obs}^{LC}$	Minimum number of shared observations between two submaps to create a loop-closure edge
$\gamma$	Constant representing the expected “sparseness” of local maps
<b>B</b>	Set of base KFs for all the observations in a KF
<b>C</b>	Set of origin KFs for all submaps of <b>B</b>
$ST.D[i][j]$	Spanning tree: Topological <i>distance</i> between KFs $i$ and $j$ . Symmetric table.
$ST.N[i][j]$	Spanning tree: The <i>next</i> edge to follow to reach $j$ from $i$ throughout the shortest path.
$ST.Reach[i]$	Spanning tree: The set of reachable KFs from $i$ within $D_{max}$
$ST.Seq[i][j]$	Spanning tree: Sequence of all edges along the shortest path from $i$ to $j$

involves having a dense graph, which is in conflict with our first desideratum.

As a trade-off, SRBA proposes a submapping approach. While *linear* RBA leads to linear graphs, ours generates a hierarchical-like lay out. With this strategy we ensure that most KFs in the graph have a degree of one, while a large number of potential observations base KFs are still available within a short topological distance.

### 5.2. Edge creation policy: submapping strategy

The *edge creation policy* (ECP) for the proposed SRBA formulation establishes a fixed number of KFs within the submaps so that when this limit is reached, a new submap is started with the new KF acting as its origin KF.

Algorithm 3 shows the process of deciding which edges must be created under such a fixed-size submapping approach. It should be mentioned that our open-source implementation allows users to redefine such an ECP to ease further research.

In any case, a new edge  $e$  is always introduced between the last origin KF  $o_{local}$  and any new KF  $n$  which is not to become the origin of a new submap. Next, we search for additional edges by checking whether the visual features produced by the front-end contain a significant number of associations with LMs whose base KFs are more distant to the current KF than  $D_{max}$ . In this case, the system determines that the camera is observing a far, already explored area, thereby detecting a loop closure and adding new edges  $e_{lc}$  to the graph (lines 25–27 of the pseudocode). We must note that there are no differences in the way that edges  $e$  and  $e_{lc}$  are inserted, no matter if they represent loop closure or simple constraints between origin KFs and submap

**Algorithm 2** `srba_define_new_keyframe`

 Worst case:  $O((\gamma N_R)^3 + N_o(D_{max} + \log N_R))$ 
**Input:**  $(z_n, \alpha_n) = \{(z_n^1, \alpha_n^1), \dots, (z_n^{N_o}, \alpha_n^{N_o})\}$ 

 ▷ Set of  $N_o$  new observations  $z_n^i$  and their data association  $\alpha_n^i$ 
**Output:** The updated, locally consistent map

```

// Update keyframes (KFs) data structures
1:  $n \leftarrow$  number of KFs in the map                                ▷ Assign a free ID to the new KF –  $O(1)$ 
2:  $KF[n] \leftarrow$  empty KF data structure                            ▷ Insertion at the end of std::map –  $O(1)$ 

// Apply edge-creation policy to decide how to handle loop closures, etc.
3:  $edge\_creation\_policy(\alpha_n, n)$  (See Algorithm 3)                ▷  $O(|C|N_R^2 \log N_R)$ 

// Update symbolic Jacobian structures
4: for each  $(z_n^i, \alpha_n^i) \in (z_n, \alpha_n)$  do                        ▷  $O(N_o(D_{max} + \log N_R))$ 
5:    $add\_observation(\underbrace{z_n^i}_{\text{obs. data}}, \underbrace{n}_{\text{observing KF}}, \underbrace{\alpha_n^i}_{\text{landmark ID}})$  (See Algorithm 6)  ▷ For each of the  $N_o$  new observations
                                                                    ▷  $O(D_{max} + \log N_R)$ 
6: end for

// Update SLAM estimation
7: edges_to_optimize  $\leftarrow$  all within a  $D_{max}$  distance from  $n$     ▷  $O(N_R)$ 
8:  $non\_linear\_optimizer(\mathbf{edges\_to\_optimize})$                         ▷  $O((\gamma N_R)^3)$ 
    
```

**Algorithm 3** `edge_creation_policy` (Submapping strategy)

 Total:  $O(|C|N_R^2 \log N_R)$ 
**Input:**
 $\alpha_n = \{\alpha_n^1, \dots, \alpha_n^{N_o}\}$ 

 ▷ IDs of all  $N_o$  observed landmarks (Data association)

 $n$ 

▷ ID of the new KF

**Output:**

New edges added to the RBA graph

```

1:  $o_{local} \leftarrow submap\_id[n]$                                 ▷ Get ID of the current submap origin –  $O(1)$ 
2:  $D_{LC} \leftarrow \underbrace{(D_{max} + 1)}_{\text{Out of range}} - \underbrace{2}_{\text{Extra edges: } n \leftrightarrow o_{local}, \text{ base KF to its origin}}$ 
                                                                    ▷ Minimum distance between submap origins for loop closure –  $O(1)$ 

// Get ordered set of base KFs with observations in  $\alpha_n$ 
3:  $\mathbf{B} \leftarrow \emptyset,$                                         ▷ Total:  $O(N_o \log |\mathbf{B}|)$ 
    $\mathbf{B}_M \leftarrow 0$ 
4: for each  $lm\_id \in \alpha_n$  do
5:    $base\_kf\_id \leftarrow$  get from  $all\_lms[lm\_id]$ 
6:    $\mathbf{B} \leftarrow \mathbf{B} \cup \{base\_kf\_id\}$                             ▷ Initialize set of KF observation bases and their multiplicity –  $O(1)$ 
                                                                    ▷ Total:  $O(N_o \log |\mathbf{B}|)$ 
7:    $\mathbf{B}_M[base\_kf\_id] \leftarrow \mathbf{B}_M[base\_kf\_id] + 1$                 ▷ Random access to vector/deque container –  $O(1)$ 
                                                                    ▷ Insert in ordered set –  $O(\log |\mathbf{B}|)$ 
                                                                    ▷ Update KF multiplicity –  $O(\log |\mathbf{B}|)$ 
8: end for

// Get ordered set of submaps with observations in  $\alpha_n$ 
9:  $\mathbf{C} \leftarrow \emptyset,$                                         ▷ Total:  $O(|\mathbf{B}| \log |\mathbf{C}|)$ 
    $\mathbf{C}_M \leftarrow 0$ 
10: for each  $base\_kf\_id \in \mathbf{B}$  do
11:    $s\_id \leftarrow submap\_id[base\_kf\_id]$ 
12:    $\mathbf{C} \leftarrow \mathbf{C} \cup \{s\_id\}$                                 ▷ Initialize set of KF submap origins and their multiplicity –  $O(1)$ 
                                                                    ▷ Total:  $O(|\mathbf{B}| \log |\mathbf{C}|)$ 
13:    $\mathbf{C}_M[s\_id] \leftarrow \mathbf{C}_M[s\_id] + \mathbf{B}_M[base\_kf\_id]$         ▷ Insert in ordered set –  $O(\log |\mathbf{C}|)$ 
                                                                    ▷ Update multiplicity –  $O(\log |\mathbf{C}|)$ 
14: end for
15:  $\mathbf{C}_S \leftarrow sort(\mathbf{C}, \mathbf{C}_M)$                                 ▷ Sort submaps by decreasing number of shared observations –  $O(|\mathbf{C}| \log |\mathbf{C}|)$ 

// Decide which KF-to-KF edges to create
16: if  $n \neq o_{local}$  then                                        ▷ Total:  $O(|C|N_R^2 \log N_R)$ 
17:    $create\_kf2kf\_edge(n \leftrightarrow o_{local})$  (See Algorithm 4)  ▷ If this KF is not the origin of the current submap
                                                                    ▷ Always connect a KF to the origin KF of its submap –  $O(N_R^2 \log N_R)$ 
18: end if
19: for each  $o_{remote} \in \mathbf{C}_S$  such that  $\mathbf{C}_M[o_{remote}] \geq N_{obs}^{LC}$  do  ▷  $O(|\mathbf{C}|)$  iterations. Total:  $O(|\mathbf{C}|N_R^2 \log N_R)$ 
20:   if  $o_{remote} \in ST.Reach[o_{local}]$  then
21:      $d \leftarrow ST.D[o_{local}][o_{remote}]$ 
22:   else
23:      $d \leftarrow \infty$ 
24:   end if
25:   if  $d \geq D_{LC}$  then
26:      $create\_kf2kf\_edge(o_{local} \leftrightarrow o_{remote})$  (See Algorithm 4)  ▷ Update KF-to-KF edge structures –  $O(N_R^2 \log N_R)$ 
27:   end if
28: end for
    
```

**Algorithm 4** create\_kf2kf\_edge

 Total:  $O(N_R^2 \log N_R)$ 
**Input:**
 $f, t$ 
 $\mathbf{p}_f^t$  (Optional; sensor model dependent)

▷ IDs of the “from” and “to” KFs

▷ Initial value of the edge inverse pose

// Allocate new kf-to-kf edge

 1:  $new\_id \leftarrow$  number of entries in  $kf2kf\_edges$ 

 2: Append new data structure with  $(f, t, new\_id, \mathbf{p}_f^t)$  at the end of  $kf2kf\_edges$ 

 3: Append a *reference* to the end of  $kf2kf\_edges$  to incidence lists for KFs  $f$  and  $t$ 

 4: Append  $new\_id$ th column to sparse Jacobian  $\partial \mathbf{h} / \partial \mathbf{p}$ 

 ▷ Total:  $O(1)$ 

 ▷ Query size of a deque container –  $O(1)$ 

 ▷ Insert at end of deque container –  $O(1)$ 

 ▷ push\_back to two containers –  $O(1)$ 

 ▷ push\_back to deque container of a symbolic CCS –  $O(1)$ 

// Update all nearby symbolic spanning trees

 5: update\_sym\_spanning\_trees( $f \leftrightarrow t$ ) (See Algorithm 5)

 ▷  $O(N_R^2 \log N_R)$ 

members. With each sequential creation of new edges, the associated shortest-path STs are updated to account for the changes introduced in the graph. Therefore, the order in which potential loop closure edges are considered (in the loop spanning lines 19–28) is important since, once an edge to a remote submap is added, other nearby submaps which were initially too far from the current KF (and could be interpreted also as loop closures), may fall within the  $D_{max}$  range, hence preventing the creation of additional edges. Thus, those submaps with the highest number of shared observations are considered first, since additional edges to them minimize the length of the pose chains from observer and base KFs, leading to more efficient nonlinear optimization steps.

In the pseudocode, this involves determining the set of base KFs associated to the current observations, as well as their multiplicity (i.e. the number of observations that belongs to each of them). Subsequently, these base KFs are grouped according to the submaps they are part of, with the aim of detecting the submaps that are affected by the current observation. Finally, we measure the distance between the origins of the involved submaps and the new node  $n$ , creating a new edge between them if such distance is over a certain value  $D_{max}$ , hence detecting the loop closure scenario.

The overall computational cost for this routine is  $O(|\mathbf{C}|N_R^2 \log N_R)$ , most of which emerges from the procedure for creating new edges, in Algorithm 4, with a cost of  $O(N_R^2 \log N_R)$ . Given that both  $|\mathbf{C}|$  and  $N_R$  can be considered to be bounded under mild assumptions, it is clear that so are these algorithms.

### 5.3. Shortest-path STs update

Regarding shortest-path STs, the SRBA approach presented in Blanco et al. (2013) creates and maintains STs for the graph up to a maximum topological distance of  $D_{max}$ , coinciding with the maximum map area that is also maintained locally consistent. There, the set of STs is implemented by means of two symbolic tables containing, for any two KFs  $i$  and  $j$ , both the topological distance in the graph between them, and the next node in the path from one to the other.

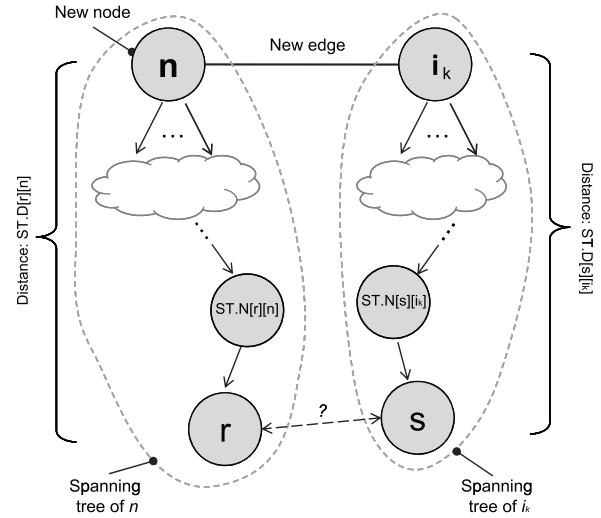


**Fig. 5.** Diagram illustrating all the elements considered in the proposed algorithm for incremental update of STs. The creation of a new edge between  $n$  and  $i_k$  may become a shortcut that changes the shortest paths between nodes at each side of the new edge.

Therefore, the shortest chain of poses between both KFs can be built by traversing these STs.

Although a ST for all of the nodes in a graph could be easily created through classic breadth-first-search algorithms (Moore, 1959), SRBA pursues the incremental build and update of both the graph and the STs as the environment is explored. Hence, the original paper proposed an incremental update algorithm for STs which we summarize next. When a new node, or KF, is added to the graph, a set of  $N$  edges connecting it to other existing KFs must be defined (although usually it will be only one). Let  $n$  be the new node in the graph and  $i_k$  the target node for one of the created edges, as shown in Figure 5. The STs for all of the nodes belonging to the STs of the involved  $n$  and  $i_k$  nodes must be checked for an update. This is performed by measuring the topological distance between any node  $r$  within the ST of  $n$  and any node  $s$  within the ST of  $i_k$ , which is determined by summing the distance between  $r$  and  $n$  (already stored in the ST of  $n$ ), the edge  $n \leftrightarrow i_k$  and the distance between the  $s$  and  $i_k$  (stored again in the ST of  $i_k$ ). If  $n$

**Algorithm 5** update\_sym\_spanning\_trees

 Worst case:  $O(N_R^2 \log N_R)$ 
**Input:**

( $i_k \leftrightarrow n$ ) $D_{max}$	▷ A new edge ▷ The maximum desired depth of STs
1: $ST_{D_{max}-1}^{i_k} \leftarrow \{\forall v/d(v, i_k) \leq D_{max} - 1\}$	▷ $O(N_R)$
2: $ST_{D_{max}}^n \leftarrow \{\forall v/d(v, n) \leq D_{max}\}$	▷ $O(N_R)$
3: <b>for each</b> $r \in ST_{D_{max}}^n$ <b>do</b>	▷ $O(N_R)$ iterations
4: <b>for each</b> $s \in ST_{D_{max}-1}^{i_k}$ <b>do</b>	▷ $O(N_R)$ iterations
5:         // New tentative distance between $r$ and $s$	
6: $d \leftarrow ST.\mathcal{D}[r] + ST.\mathcal{D}[i_k][s] + 1$	
7: <b>if</b> ( $s \in ST.\text{Reach}[r]$ <b>and</b> $d < ST.\mathcal{D}[r][s]$ ) <b>or</b> ( $s \notin ST.\text{Reach}[r]$ <b>and</b> $d \leq D_{max}$ ) <b>then</b>	▷ $O(\log N_R)$ ▷ $O(\log N_R)$
8:             // Shorter or new path found. Update trees:	
9: $ST.\mathcal{D}[r][s] \leftarrow d$	
10: $ST.\mathcal{N}[r][s] \leftarrow \begin{cases} i_k & r = n \\ ST.\mathcal{N}[r][n] & r \neq n \end{cases}$	
11: $ST.\mathcal{D}[s][r] \leftarrow d$	▷ $O(\log N_R)$
12: $ST.\mathcal{N}[s][r] \leftarrow \begin{cases} n & s = i_k \\ ST.\mathcal{N}[s][i_k] & s \neq i_k \end{cases}$	
13: <b>end if</b>	
14: <b>end for</b>	
15: <b>end for</b>	

and  $i_k$  were not already in each other's ST and the resulting distance is  $D_{max}$  or less, both STs are updated to account for this new relation. Otherwise, if there was already a path between such nodes, their STs are only updated if the new path is shorter than the existing one. This process has to be repeated for all of the created new edges, and it is summarized in Algorithm 5. A careful analysis of its computational cost, including access and creation of data structures, reveals a worst-case complexity of  $O(N_R^2 \log N_R)$ , with  $N_R$  being the maximum number of reachable KFs for a given  $D_{max}$  and which is reasonable to consider bounded for any large and complex map, as long as redundant KFs are not continuously added to the map for the same physical area.

#### 5.4. Observation insertion

Finally, lines from 4 to 6 in Algorithm 2 refer to the insertion of the current set of observations into the SRBA-based SLAM system, a process summarized in Algorithm 6.

For each individual observation, the general procedure involves creating and appending new structures to both the system observations and LMs containers (the latter just in case we are observing a new LM). This is performed in  $O(1)$ .

Subsequently, we proceed to update the system sparse Jacobian structure, which is stored in two separate parts: the Jacobian with respect to the edges ( $\partial \mathbf{h} / \partial \mathbf{p}$ ) and with respect to the LMs ( $\partial \mathbf{h} / \partial \mathbf{x}$ ). For the former, we need to update all of the matrix columns associated to the edges in the chain of poses between the current *observer* KF and the observation base KF, by appending a new block to each one of them (refer to Figure 6 for an example of a Jacobian matrix). In this situation, the strategy followed by SRBA reduces the number of entries that must be updated since the traversed paths involves fewer edges, hence keeping the Jacobian

sparser than standard RBA approaches. The complexity of updating this part of the Jacobian is  $O(P + \log M)$ , with  $P$  being the number of edges between the above-mentioned KFs and  $M$  the number of nodes stored in the system ST. In the worst case we have that  $M = N_R$  and  $P = D_{max}$ , i.e. the number of reachable nodes in each ST and the maximum topological distance allowed for the ST, respectively.

Updating the Jacobian with respect to the LMs is much simpler and can be performed in  $O(1)$ .

#### 5.5. Least-squares optimization

The graph optimization is performed by an iterative Levenberg–Marquardt algorithm, which is a slight variation of the Gauss–Newton procedure that minimizes the reprojection error of the observed LMs explained in Section 4.2 for the visual odometry method. In this case, though, minimizing the cost function in Equation (6) achieves the joint estimation of both the poses of the cameras  $\mathbf{p}$  that captured the images (i.e. the KFs) and the LM positions  $\mathbf{x}$ . This leads to the following linear equation, equivalent to Equation (8) but taking into account the whole system:

$$(\mathbf{H} + \lambda \mathbf{I}) \Delta \mathbf{s} = -\mathbf{g} \quad (12)$$

where  $\mathbf{H}$  and  $\mathbf{g}$  stand for the approximate Hessian matrix and the gradient of the prediction function, respectively,  $\Delta \mathbf{s}$  standing for the incremental change in the system unknowns  $\mathbf{s} = (\mathbf{p}, \mathbf{x})$  and  $\lambda$  a scalar parameter of the Levenberg–Marquardt algorithm. Note that part of the state vector, in particular, all of the relative poses, has the non-Euclidean topology of  $\mathbf{SE}(3)$ . Therefore, we have followed the common practice of formulating Equation (12) in the error state formulation (see, e.g., Grisetti et al., 2010), such that increments on  $\mathfrak{se}(3)$  are obtained from the linear solver, then added as corrections through the corresponding Lie

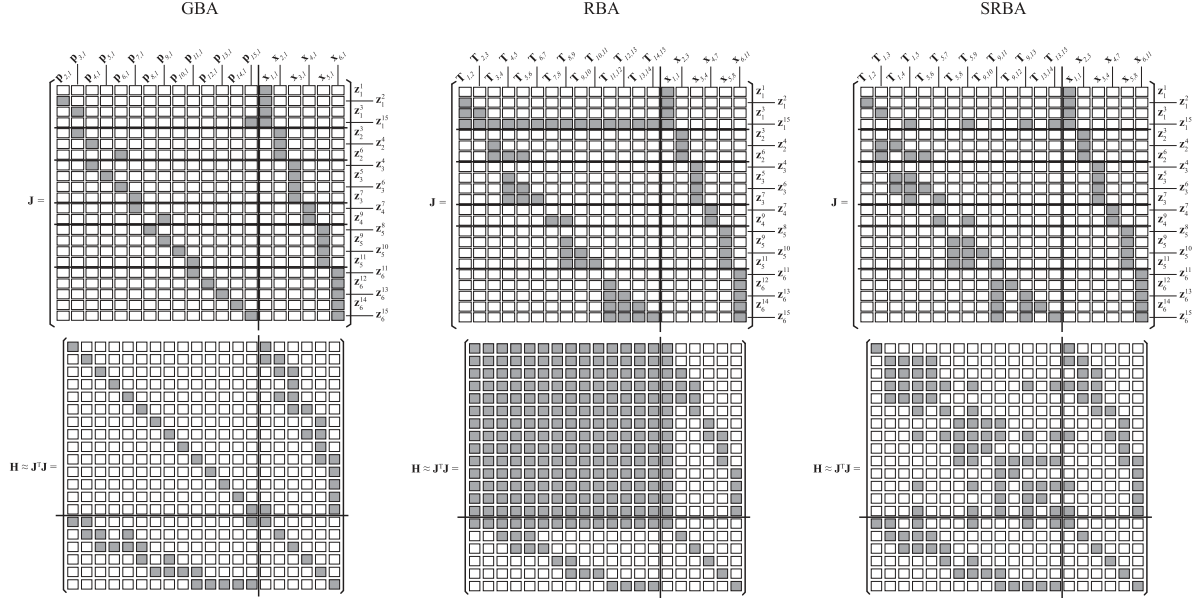


**Fig. 6.** Sparsity pattern of Jacobian and Hessian matrices under the GBA, linear RBA and SRBA approaches for the scenario shown in Figure 3. Gray squares represent dense blocks within the matrix.

---

**Algorithm 6** `add_observation`

Total:  $O(D_{max} + \log N_R)$

**Input:**

$\mathbf{z}$  ▷ Observation data  
 $kf\_id$  ▷ ID of the observing KF  
 $lm\_id$  ▷ ID of the observed landmark

// Observation data housekeeping

1:  $obs\_id \leftarrow$  overall number of observations in  $all\_obs$  ▷ Query size of a vector/deque container –  $O(1)$   
 2: Append  $(\mathbf{z}, kf\_id, lm\_id)$  at the end of  $all\_obs$  ▷ push\_back on vector/deque container –  $O(1)$

// Handle new landmarks

3: **if**  $lm\_id \notin all\_lms$  **then** ▷ Test for existence flag in a vector/deque container –  $O(1)$   
 4:  $all\_lms[lm\_id] \leftarrow$  new  $kf2lm$  edge data structure ▷ Create new  $kf2lm$  edge – Amortized  $O(1)$   
 5: Append column to sparse Jacobian  $\partial \mathbf{h} / \partial \mathbf{x}$  ▷ push\_back to deque container of a symbolic CCS –  $O(1)$   
 6: Update bimap of column indices in  $\partial \mathbf{h} / \partial \mathbf{x} \leftrightarrow$  landmark indices ▷ With map\_as\_vector can be done in  $O(1)$   
 7: **end if**

8:  $base\_id \leftarrow$  get from  $all\_lms[lm\_id]$  ▷ Random access to vector/deque container –  $O(1)$   
 9: Append a reference to  $all\_lms[lm\_id]$  to the incidence list for  $kf\_id$  ▷  $O(1)$

// Update symbolic linear system ( $\partial \mathbf{h} / \partial \mathbf{p}$  part)

10: **if**  $base\_id \neq kf\_id$  **then** ▷ Total:  $O(D_{max} + \log N_R)$   
 11:  $obs\_edges \leftarrow ST.Seq$   $[base\_id]$   $[kf\_id]$  ▷ Observations from the base KF introduce no blocks to this Jacobian  
     Access in  $O(1)$  Access in  $O(\log N_R)$  ▷ Retrieve list of  $\leq D_{max}$  observed  $kf2kf$  edges from spanning trees –  $O(\log N_R)$   
 12: **for each**  $kf2kf\_edge\_id \in obs\_edges$  **do** ▷  $O(D_{max})$  iterations  
 13:  $col \leftarrow [\partial \mathbf{h} / \partial \mathbf{p}].cols$   $[kf2kf\_edge\_id]$  ▷ Retrieve symbolic sparse column –  $O(1)$   
     Access to deque in  $O(1)$   
 14:  $col$   $[obs\_id] \leftarrow$  reference to observation data and other symbolic data ▷ Typically, an insertion at the end of map – Typ.  $O(1)$   
     Insert into map  
 15: **end for**  
 16: **end if**

// Update symbolic linear system ( $\partial \mathbf{h} / \partial \mathbf{x}$  part)

17:  $kf2lm\_edge\_id \leftarrow$  bimap from  $lm\_id$  ▷ Total:  $O(1)$   
 18:  $col \leftarrow [\partial \mathbf{h} / \partial \mathbf{x}].cols$   $[kf2lm\_edge\_id]$  ▷ With map\_as\_vector can be done in  $O(1)$   
     Access to deque in  $O(1)$  ▷ Retrieve symbolic sparse column –  $O(1)$   
 19:  $col$   $[obs\_id] \leftarrow$  reference to observation data and other symbolic data ▷ Typically, an insertion at the end of map – Typ.  $O(1)$   
     Insert into map

---

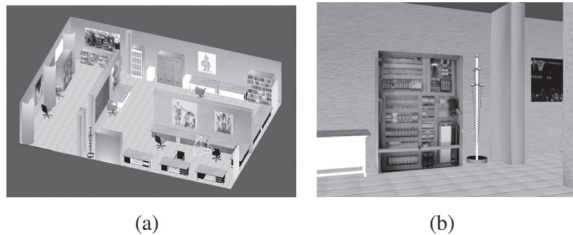


**Fig. 7.** (a) Plan and (b) example image of the synthetic dataset.

group exponential map. For further mathematical details, the interested reader could refer to the technical report in Blanco (2010).

The sparsity of the Jacobian matrices, and hence the Hessian, plays here an important role in terms of computational burden, favoring SRBA by improving its performance in comparison to the standard, linear RBA method. Figure 6 represents the sparsity patterns of such matrices for the example proposed in Figure 3 under the GBA, RBA and SRBA formulations. In comparison to those for the GBA and standard RBA approaches, it can be noted that SRBA falls in between both formulations, yielding sparser matrices than RBA but denser than GBA.

## 6. Experimental results

Experiments in both indoor and outdoor environments are presented in this section in order to validate the proposed system.

### 6.1. Synthetic images dataset

In our first experiment, we have moved a virtual stereo camera through a synthetic office-like environment created with the 3D design software Blender while capturing stereo images to form a dataset of synthetic images. A representation of such environment and an example of the captured images are shown in Figure 7. The use of a virtual environment to test our approach is motivated here by the fact that the camera movement is known beforehand, hence making a *ground truth* available for the camera path.

As presented previously, the main advantage of our relative representation is that the time spent in creating and inserting new KFs (including the creation of the Hessian matrix and the subsequent optimization process) remains bounded, unlike the global approach. This is a consequence of the smaller matrices employed in our method due to the existence of submaps and a limit depth for graph optimization. To test this, we have employed the same dataset as input for both our SRBA-based approach and a pure global one (GBA).

In this sense, a performance comparison can be seen in Figure 8, where the KF creation time (including the graph optimization step) is plotted for every KF defined during the experiment under both approaches. Please, note that we

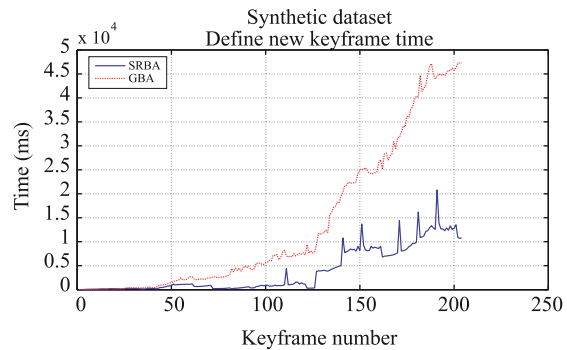


**Fig. 8.** Inserting new KF time (including graph optimization) comparison for SRBA (blue solid line) and GBA (red dashed line) for the synthetic dataset.

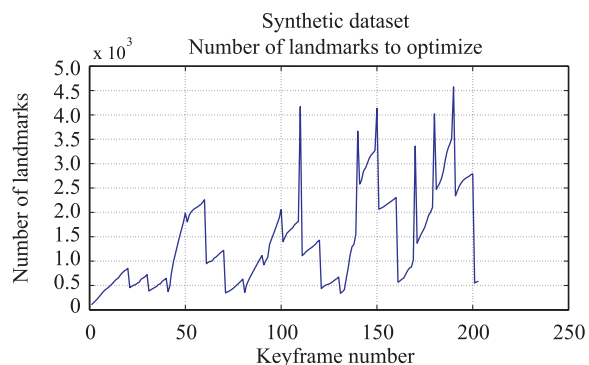


**Fig. 9.** Number of landmarks to optimize with SRBA for the synthetic dataset.

have not performed any optimization in our code to pursue efficient performance, hence the mentioned plot should be understood as a mere relative comparison between both techniques, disregarding the absolute time values. Figure 9 also presents the number of LM positions that are optimized at each KF insertion for the SRBA method, showing that it remains bounded over time, unlike global approaches.

Finally, we present in Figure 10 a comparison between the estimated camera trajectory and the ground truth. The path of the camera has been obtained through a final full optimization of the graph built through our method in order to determine both KF poses and LM positions within a unique global reference system whose origin is set at the first camera position. We also present in Figure 11 the errors at the estimated camera positions associated to all the KFs.

It has to be noted that, although the creation of an unique global map cannot be considered part of our SRBA formulation, the presented path comparison and accuracy results represent indicators about the suitability of our method to store and manage enough information to create a global map in case that the application demands it. At the same time, it allows a more efficient way of estimating a camera trajectory while creating a map of the environment which is locally consistent and useful enough for many applications.

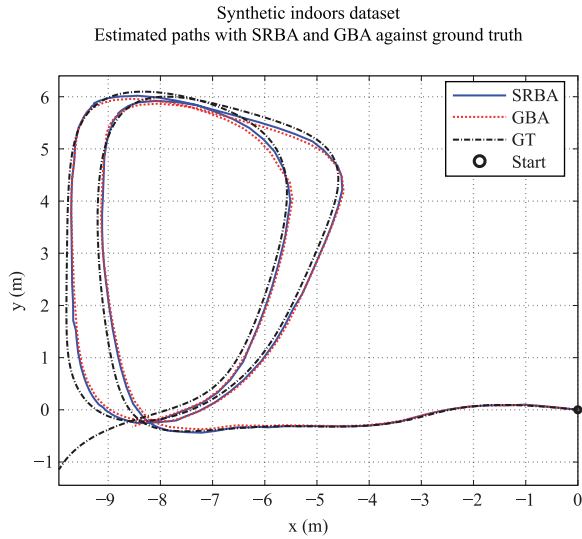


**Fig. 10.** Estimated paths for the synthetic dataset with SRBA (blue solid line) and GBA (red dashed line). Ground truth is also represented (black dashed-dotted line).

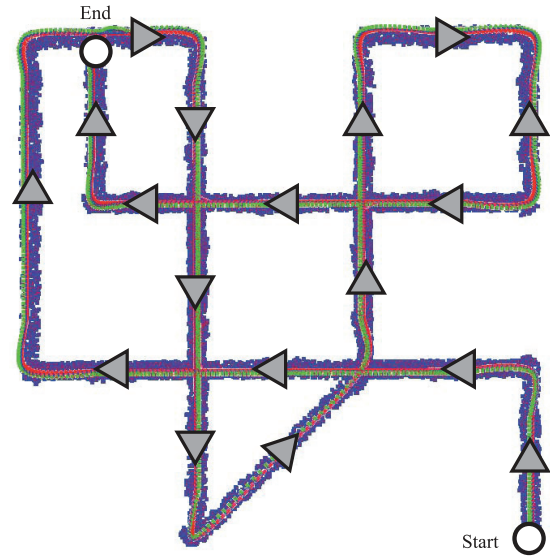


**Fig. 12.** Path followed by the robot in the synthetic dataset used to compare SRBA with linear RBA. Observed visual LMs are represented as blue dots.

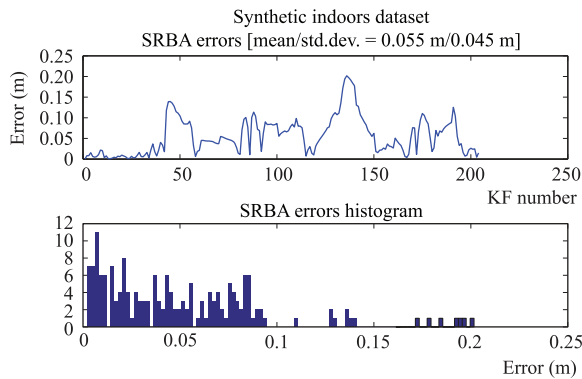


**Fig. 11.** Absolute error and histogram of errors for our SRBA-based method with respect to the ground truth for the synthetic dataset.

Finally, aiming at comparing the performance of standard RBA and our approach, we present another experiment with a synthetic dataset generated with the freely available Recursive World Toolkit (RWT; <https://github.com/jlblancoc/recursive-world-toolkit>). In this case, we simulate the observations of a stereo camera moving along a corridor-like environment, which is populated with randomly-distributed 3D LMs, and includes several loops, as shown in Figure 12. We subsequently compare the sparsity of the Hessian matrix  $s_H$  at every KF insertion (and graph optimization), defined, in this experiment, as the ratio between the non-zero entries of the matrix and the total number of elements. This comparison, together with the time spent in the graph optimization for both methods, can be seen in Figure 13. Note the higher matrix sparsity in the SRBA approach, leading to smaller computational times including at loop closures.

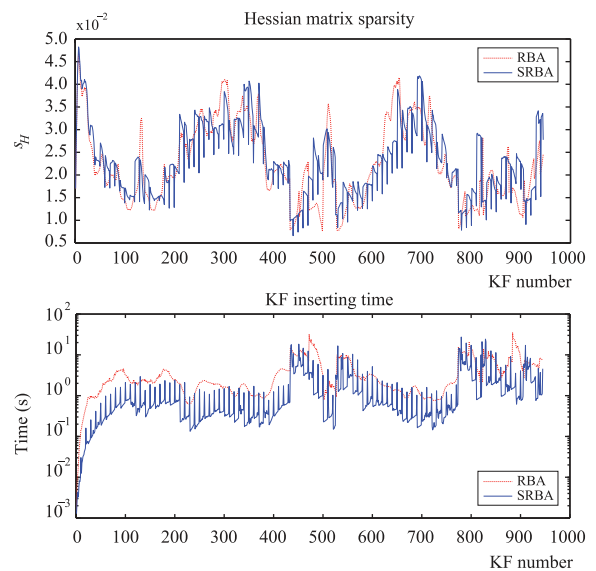


**Fig. 13.** Performance comparison for classic (linear) RBA (dashed red line) and SRBA (solid blue line). (Top) Hessian matrix sparsity as the ratio of non-zero matrix blocks and (bottom) time spent in optimizing the graph for each KF insertion ( $y$ -axis is logarithmic). In both graphs, smaller is better.

Moreover, we present in Figure 14 the number of KFs and LMs that are updated in each KF insertion for both approaches, as a measure of the *size* of the local map that is updated, and hence maintained consistent, after each graph optimization. Notice that, overall, our proposal keeps consistency for larger local maps than linear RBA.



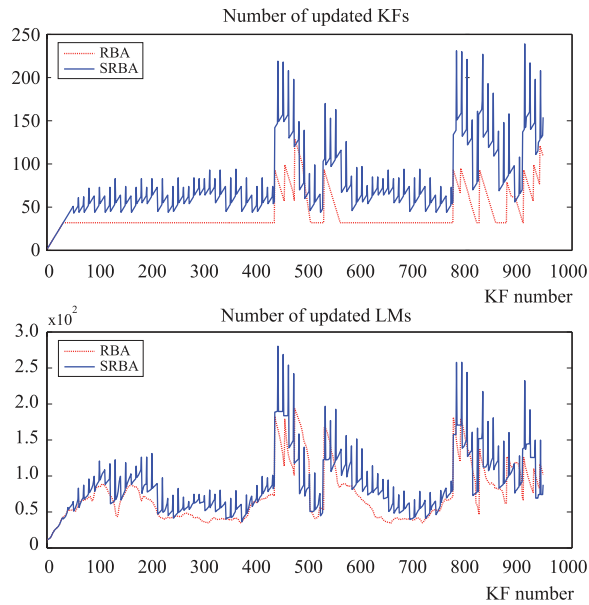


**Fig. 14.** Number of (top) KFs and (bottom) LMs that are updated at each KF insertion (involving graph optimization) for standard RBA (dashed red line) and SRBA (solid blue line). In both graphs, larger is better.

### 6.2. Real indoors dataset

In this second experiment we have tested our method against a real image dataset gathered with Sancho (Gonzalez et al., 2009), one of our mobile robots, while navigating through our laboratory following a trajectory that includes a loop. Unfortunately no ground truth could be provided for this experiment since no other sensors were available on the robot at that time. Therefore, both the obtained map and the robot path can only be validated by means of visual inspection.

Figure 15 presents the timing comparison when creating new KFs under both our SRBA-based approach and a global one. A spike can be noted in SRBA insertion time around KF#360 due the detection of loop closure. At that time, the number of KFs included into the graph optimization increases significantly, since the *old* submaps involved in the closure are also included together with the most recent ones. Finally, regarding the time absolute values, similar considerations to those mentioned in the previous experiment must be taken into account here. An example of the images employed in this experiment can be found in Figure 16 while Figure 17 shows the estimated trajectory of the camera for both methods.

### 6.3. Real outdoors dataset

Finally, we have employed two outdoor datasets to test our method under more challenging conditions. In concrete we use one of our published stereo datasets (Blanco-Claraco et al., 2014) (referred as MAPIR dataset from now on), and

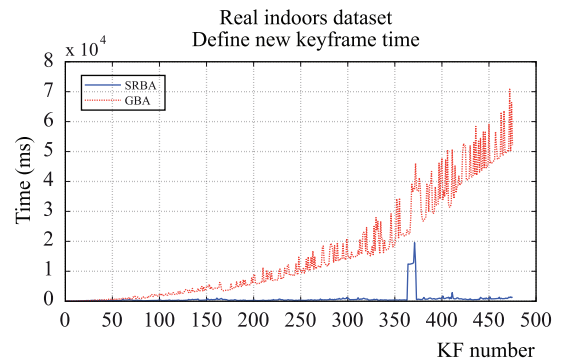


**Fig. 15.** Inserting new KF time (including graph optimization) comparison for SRBA (blue solid line) and GBA (red dashed line) for the real indoors dataset.



**Fig. 16.** Example images for the real indoors dataset.

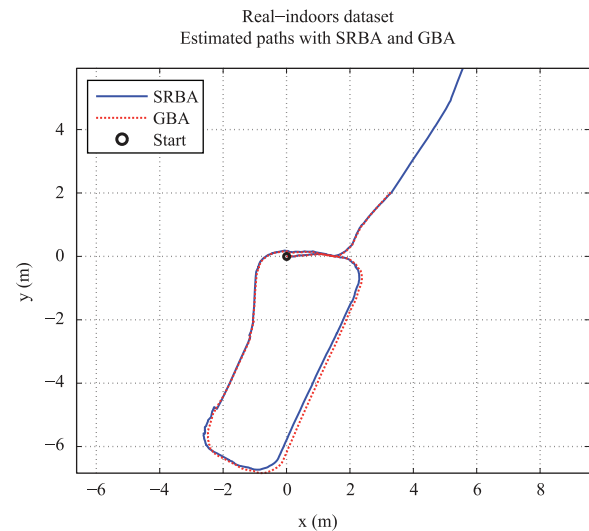


**Fig. 17.** Estimated paths for the real indoors dataset with SRBA (blue solid line) and GBA (red dashed line).

one of the *road* datasets from the KITTI Vision Benchmark Suite (Fritsch et al., 2013; Geiger et al., 2012).

First, we have chosen the fragment number 7 of the MAPIR outdoors dataset, which contains a  $\sim 0.7$  km long loop within an urban scenario gathered by an on-board stereo camera placed on a standard car. The positioning information provided by a standard differential GPS device is considered the ground truth for this experiment.

The timing comparison when creating new KFs for this experiment is shown in Figure 18. Note that due to the size of the resulting map, with a total amount of more than

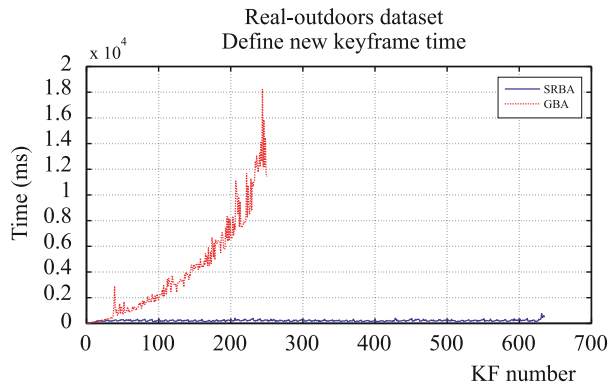


**Fig. 18.** Inserting new KF time (including graph optimization) comparison for SRBA (blue solid line) and GBA (red dashed line) for the real outdoors dataset.

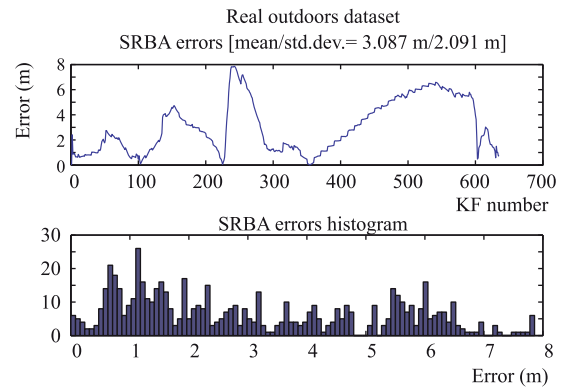


**Fig. 20.** Absolute error and histogram of errors for the SRBA method with respect to the ground truth for the real outdoors dataset.

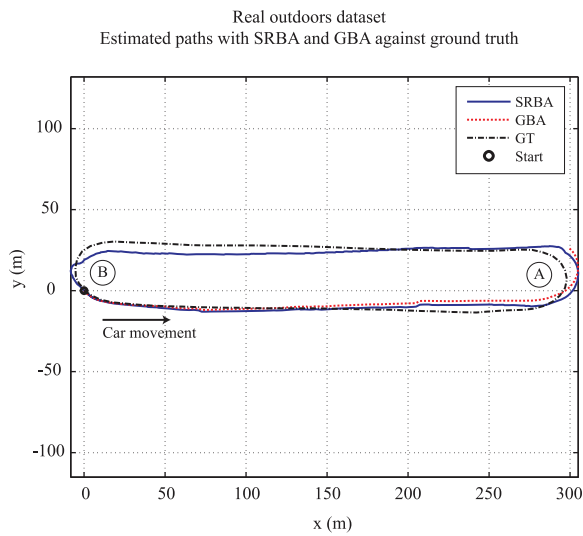


**Fig. 19.** Estimated paths for the real outdoors dataset with SRBA (blue solid line) and GBA (red dashed line). Ground truth is also represented (black dashed-dotted line).

110,000 LMs, the time spent when inserting KFs by our GBA implementation rapidly becomes excessive. Therefore, beyond the insertion of KF#250, GBA time values are no longer shown in the plot. The small peak that appears around the KF#630 for the SRBA-method is due to the loop closure detection.

One of the main drawbacks of this dataset stands on the relatively small baseline of the employed stereo camera ( $\sim 12$  cm), which makes difficult the estimation of distant points' 3D position. Still, the achieved results can be considered to be promising. A comparison between the estimated camera paths and the GPS-based ground truth is shown in Figure 19 while the errors between both trajectories are presented in Figure 20. The camera path estimated by the GBA method is only depicted up to KF#250.

Moreover, it has to be noted that, in some areas of this dataset, the environment is not static due to the presence of moving cars and/or pedestrians. Since our system works

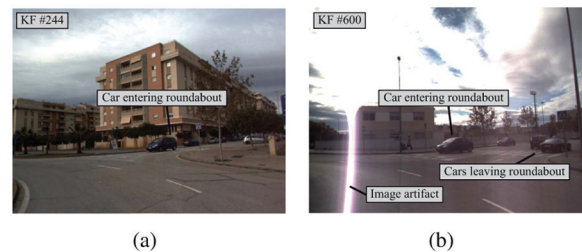


**Fig. 21.** Example of problematic images for the real outdoors dataset. (a) A car entering a roundabout and (b) image artifact and moving cars at a roundabout.

under the assumption of a non-dynamic environment, this leads to large inaccuracies in the camera path estimation. Hence, manual assistance has been required in such areas. In particular, a car approaching the roundabout marked as “A” in Figure 19 and the presence of some cars entering and leaving the roundabout marked as “B” in the same figure (nearly the end of the trajectory) are the specific areas where capturing keypoints on moving objects has been avoided. Example images of these situations are shown in Figure 21. Finally, the presence of image artifacts due to direct sunlight (refer to Figure 21(b)) has also been managed in a similar way at the very end of the dataset.

Finally, we have also taken segment 7 from the KITTI's road datasets to test our approach. This segment contains a set of 1100 stereo images of size  $1226 \times 370$  pixels (refer to Figure 22 for an example image) captured by a car while moving along a  $\sim 0.7$  km long trajectory and performing a loop. In this case, the stereo camera baseline is significantly wider than the dataset employed in the previous experiment and, similarly to it, ground truth is available for this dataset.

Again, we have measured the insertion time for new KFs (including graph optimization) for both the GBA and the SRBA approaches, presenting the results in Figure 23. Note that, similarly to the previous experiment, the high number of LMs in the map prevent the process of inserting new KFs for our GBA implementation to perform in reasonable time. Loop closure detection is achieved near to KF#400 for the



**Fig. 22.** Example image for the KITTI outdoors dataset.

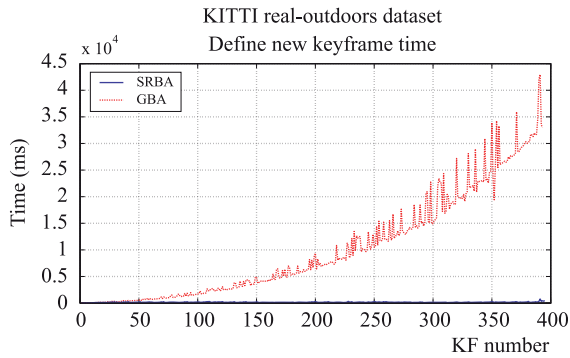


**Fig. 23.** Inserting new KF time (including graph optimization) comparison for SRBA (blue solid line) and GBA (red dashed line) for the KITTI real outdoors dataset.

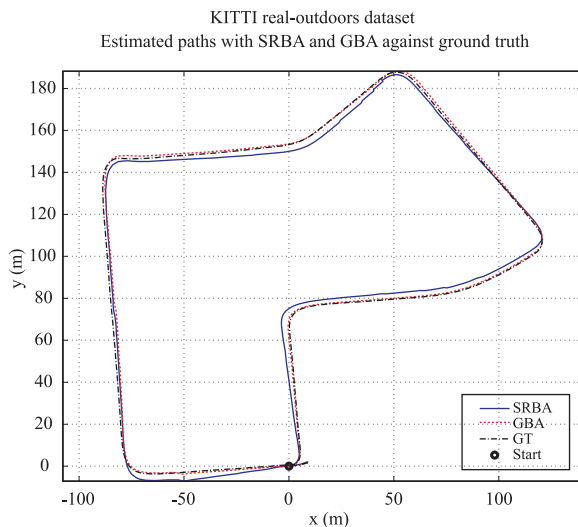


**Fig. 24.** Estimated paths for the KITTI real outdoors dataset with SRBA (blue solid line) and GBA (red dashed line). Ground truth is also represented (black dashed-dotted line).

SRBA approach, hence the small peak shown in the figure at that point.

The paths estimated by both methods are compared against the provided ground truth as shown in Figure 24. The graph built contained  $\sim 400$  KFs for the whole trajectory and the resulting map was composed by more than 36,000 LMs. Finally, the evolution and the histogram of the errors committed by the SRBA method with respect to the ground truth are presented in Figure 25. A video showing SRBA operation for this experiment can be found at <https://goo.gl/1Ap4p9>.

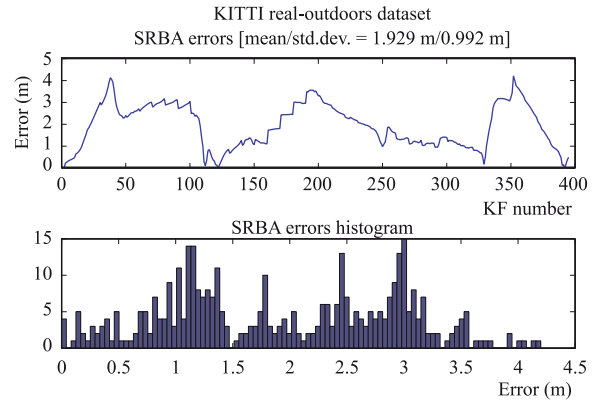


**Fig. 25.** Absolute error and histogram of errors for the SRBA method with respect to the ground truth for the KITTI real outdoors dataset.

## 7. Conclusion

This paper has addressed the development of a blended relative–global approach to BA, coined SRBA, which allows for a continuum of strategies ranging from classic linear RBA to hybrid submapping with local maps. This flexibility leads to graphs that can be optimized more efficiently than those built as previously reported in the literature, ensuring a bounded-time operation even in the presence of loop closures, regardless of their size.

In this work we have extended the preliminary description of SRBA in Blanco et al. (2013), proven its constant-time nature by providing in-depth listings for the most important algorithms, and validated its performance in the context of stereo visual SLAM. For that, we have developed a complete system combining a front-end that integrates several state-of-the-art computer vision techniques and an SRBA-based back-end that operates as graph optimizer. The presented front-end relies on ORB features as image keypoints and computes camera ego-motion through a visual odometry method which is robust against the presence of outliers. Data association, in turn, is assisted by a bag-of-words built upon ORB binary descriptors that restricts the search area when looking for loop closures.

A set of experiments in both indoor and outdoor conditions is presented to demonstrate the capabilities of our method when tackling with visual SLAM in comparison with other BA approaches in terms of accuracy and efficiency. Future works include introducing further optimizations in our SRBA implementation, as well as analyzing and introducing more graph maintenance operations to improve its suitability as a long-term SLAM solution.

## Note

1. The C++ source code for the front-end and back-end can be found at <https://github.com/famoreno/srba-stereo-slam> and at <https://github.com/MRPT/srba>, respectively.

## Funding

This work has been partially funded by the Spanish *Ministerio de Ciencia e Innovación* under the projects “TAROTH: New developments toward a Robot at Home” (contract number DPI 2011-25483) and “PROMOVE: Advances in mobile robotics for promoting independent life of elders” (contract number DPI 2014-55826-R). Both projects are co-funded by *Fondo Europeo de Desarrollo Regional (FEDER)*.

## References

- Agarwal S, Snavely N, Seitz SM and Szeliski R (2010) Bundle adjustment in the large. In: *European conference on computer vision (ECCV)*. New York: Springer, pp. 29–42.
- Anderson S, MacTavish K and Barfoot TD (2015) Relative continuous-time SLAM. *The International Journal of Robotics Research* 34(12): 1453–1479.
- Blanco J, Fernandez-Madriral J and Gonzalez J (2008) Towards a unified Bayesian approach to hybrid metric-topological SLAM. *IEEE Transactions on Robotics* 24(2): 259–270.
- Blanco J, González J and Fernández-Madriral JA (2010) Optimal filtering for non-parametric observation models: applications to localization and SLAM. *The International Journal of Robotics Research* 29(14): 1726–1742.
- Blanco JL (2010) A tutorial on SE(3) transformation parameterizations and on-manifold optimization. Technical report, University of Malaga.
- Blanco JL, González-Jiménez J and Fernández-Madriral JA (2012) An alternative to the Mahalanobis distance for determining optimal correspondences in data association. *IEEE Transactions on Robotics* 28(4): 980–986.
- Blanco JL, González-Jiménez J and Fernández-Madriral JA (2013) Sparser relative bundle adjustment (srba): constant-time maintenance and local optimization of arbitrarily large maps. In: *IEEE international conference on robotics and automation (ICRA)*. IEEE, pp. 70–77.
- Blanco-Claraco JL (2013) User guide for `libmrpt-srba`: A generic c++ framework for relative bundle adjustment (RBA). Available at: <http://www.mrpt.org/srba>.
- Blanco-Claraco JL, Moreno-Dueñas FA and González-Jiménez J (2014) The Málaga urban dataset: High-rate stereo and lidar in a realistic urban scenario. *The International Journal of Robotics Research* 33(2): 207–214.
- G. Bradski and A. Kaehler, “Learning OpenCV: Computer Vision with the OpenCV Library,” in O’Reilly Media, Inc., 2008, pp. 415–453.
- Calonder M, Lepetit V, Strecha C and Fua P (2010) Brief: Binary robust independent elementary features. In: *European conference on computer vision (ECCV)*. New York: Springer, pp. 778–792.
- Civera J, Davison A and Montiel J (2007) Inverse depth to depth conversion for monocular SLAM. In: *IEEE international conference on robotics and automation (ICRA)*. IEEE, pp. 2778–2783.
- Concha A and Civera J (2015) An evaluation of robust cost functions for RGB direct mapping. In: *European conference on mobile robotics (ECMR15)*.
- Davis TA (2006) *Direct methods for sparse linear systems*, volume 2. Philadelphia, PA: Society for Industrial and Applied Mathematics (SIAM).
- Eade E and Drummond T (2008) Unified loop closing and recovery for real time monocular SLAM. In: *Proceedings of the British machine vision conference*. BMVA Press, pp. 6.1–6.10. DOI: 10.5244/C.22.6.
- Fritsch J, Kuehnl T and Geiger A (2013) A new performance measure and evaluation benchmark for road detection algorithms. In: *International conference on intelligent transportation systems (ITSC)*. IEEE, pp. 1693–1700.
- Galvez-Lopez D and Tardos JD (2012) Bags of binary words for fast place recognition in image sequences. *IEEE Transactions on Robotics* 28(5): 1188–1197.
- Geiger A, Lenz P and Urtasun R (2012) Are we ready for autonomous driving? The KITTI vision benchmark suite. In: *IEEE conference on computer vision and pattern recognition (CVPR)*. IEEE, pp. 3354–3361.
- Gonzalez J, Galindo C, Blanco J, Fernandez-Madriral J, Arevalo V and Moreno F (2009) Sancho, a fair host robot. A description. In: *IEEE international conference on mechatronics (ICM)*, pp. 1–6. DOI: 10.1109/ICMECH.2009.4957181.
- Grisetti G, Kummerle R, Stachniss C, Frese U and Hertzberg C (2010) Hierarchical optimization on manifolds for online 2D and 3D mapping. In: *2010 IEEE international conference on robotics and automation (ICRA)*. IEEE, pp. 273–278.
- Hamming RW (1950) Error detecting and error correcting codes. *Bell System Technical Journal* 29(2): 147–160.
- Hartley R and Kahl F (2007) Optimal algorithms in multiview geometry. In: Yagi Y, Kang S, Kweon I and Zha H (eds), *Computer vision – ACCV (Lecture Notes in Computer Science*, vol. 4843). Berlin: Springer, pp. 13–34.
- Huber P and Ronchetti E (1981) *Robust statistics*, volume 1. Wiley Online Library.
- Kaess M, Johannsson H, Roberts R, Ila V, Leonard JJ and Dellaert F (2012) iSAM2: Incremental smoothing and mapping using the Bayes tree. *The International Journal of Robotics Research* 31(2): 216–235.
- Kaess M, Ranganathan A and Dellaert F (2008) iSAM: Incremental smoothing and mapping. *IEEE Transactions on Robotics* 24(6): 1365–1378.
- Klein G and Murray D (2007) Parallel tracking and mapping for small AR workspaces. In: *IEEE/ACM international symposium on mixed and augmented reality (ISMAR)*. IEEE, pp. 225–234.
- Konolige K and Agrawal M (2008) FrameSLAM: From bundle adjustment to real-time visual mapping. *IEEE Transactions on Robotics* 24(5): 1066–1077.
- Lim J, Frahm JM and Pollefeys M (2011) Online environment mapping. In: *IEEE conference on computer vision and pattern recognition (CVPR)*. IEEE, pp. 3489–3496.
- Moore EF (1959) *The shortest path through a maze*. Bell Telephone System.
- Moreno FA, Blanco JL and Gonzalez J (2009) Stereo vision specific models for particle filter-based SLAM. *Robotics and Autonomous Systems* 57(9): 955–970.
- Moreno FA, Blanco JL and González-Jiménez J (2013) Erode: An efficient and robust outlier detector and its application to stereovision odometry. In: *IEEE international conference on robotics and automation (ICRA)*. IEEE, pp. 4691–4697.
- Mur-Artal R, Montiel J and Tardos JD (2015) ORB-SLAM: a versatile and accurate monocular SLAM system. *IEEE Transactions on Robotics* 31(5): 1147–1163.
- Rosten E and Drummond T (2006) Machine learning for high-speed corner detection. In: *European conference on computer*

- Rublee E, Rabaud V, Konolige K and Bradski G (2011) ORB: an efficient alternative to SIFT or SURF. In: *IEEE international conference on computer vision (ICCV)*. IEEE, pp. 2564–2571.
- Sibley D, Mei C, Reid I and Newman P (2009) Adaptive relative bundle adjustment. In: *Robotics: science and systems*, volume 32. Cambridge, MA: MIT Press, pp. 33–40.
- Sibley G (2009) Relative bundle adjustment. Technical Report 2307(09), Department of Engineering Science, Oxford University.
- Sibley G, Matthies L and Sukhatme G (2010a) Sliding window filter with application to planetary landing. *Journal of Field Robotics* 27(5): 587–608.
- Sibley G, Mei C, Reid I and Newman P (2010b) Vast-scale outdoor navigation using adaptive relative bundle adjustment. *The International Journal of Robotics Research* 29(8): 958–980.
- Strasdat H, Montiel J and Davison AJ (2010) Real-time monocular SLAM: Why filter? In: *IEEE international conference on robotics and automation (ICRA)*. IEEE, pp. 2657–2664.
- Strasdat H, Montiel JM and Davison AJ (2012) Visual SLAM: why filter? *Image and Vision Computing* 30(2): 65–77.
- Thrun S, Burgard W and Fox D (2005) *Probabilistic Robotics*. Cambridge, MA: The MIT Press.
- Triggs B, McLauchlan PF, Hartley RI and Fitzgibbon AW (2000) Bundle adjustment - a modern synthesis. In: *Vision algorithms: theory and practice*. New York: Springer, pp. 298–372.
- Wolf J, Burgard W and Burkhardt H (2002) Robust vision-based localization for mobile robots using an image retrieval system based on invariant features. In: *Proceedings of the IEEE international conference on robotics and automation (ICRA)*, volume 1. IEEE, pp. 359–365.